

# Impact of Network Activity on the Integrative Properties of Neocortical Pyramidal Neurons In Vivo

ALAIN DESTEXHE AND DENIS PARÉ

*Laboratoire de Neurophysiologie, Département de Physiologie, Université Laval, Québec G1K 7P4, Canada*

**Destexhe, Alain and Denis Paré.** Impact of network activity on the integrative properties of neocortical pyramidal neurons in vivo. *J. Neurophysiol.* 81: 1531–1547, 1999. During wakefulness, neocortical neurons are subjected to an intense synaptic bombardment. To assess the consequences of this background activity for the integrative properties of pyramidal neurons, we constrained biophysical models with in vivo intracellular data obtained in anesthetized cats during periods of intense network activity similar to that observed in the waking state. In pyramidal cells of the parietal cortex (area 5–7), synaptic activity was responsible for an approximately fivefold decrease in input resistance ( $R_{in}$ ), a more depolarized membrane potential ( $V_m$ ), and a marked increase in the amplitude of  $V_m$  fluctuations, as determined by comparing the same cells before and after microperfusion of tetrodotoxin (TTX). The model was constrained by measurements of  $R_{in}$ , by the average value and standard deviation of the  $V_m$  measured from epochs of intense synaptic activity recorded with KAc or KCl-filled pipettes as well as the values measured in the same cells after TTX. To reproduce all experimental results, the simulated synaptic activity had to be of relatively high frequency (1–5 Hz) at excitatory and inhibitory synapses. In addition, synaptic inputs had to be significantly correlated (correlation coefficient  $\sim 0.1$ ) to reproduce the amplitude of  $V_m$  fluctuations recorded experimentally. The presence of voltage-dependent  $K^+$  currents, estimated from current-voltage relations after TTX, affected these parameters by  $<10\%$ . The model predicts that the conductance due to synaptic activity is 7–30 times larger than the somatic leak conductance to be consistent with the approximately fivefold change in  $R_{in}$ . The impact of this massive increase in conductance on dendritic attenuation was investigated for passive neurons and neurons with voltage-dependent  $Na^+/K^+$  currents in soma and dendrites. In passive neurons, correlated synaptic bombardment had a major influence on dendritic attenuation. The electrotonic attenuation of simulated synaptic inputs was enhanced greatly in the presence of synaptic bombardment, with distal synapses having minimal effects at the soma. Similarly, in the presence of dendritic voltage-dependent currents, the convergence of hundreds of synaptic inputs was required to evoke action potentials reliably. In this case, however, dendritic voltage-dependent currents minimized the variability due to input location, with distal apical synapses being as effective as synapses on basal dendrites. In conclusion, this combination of intracellular and computational data suggests that, during low-amplitude fast electroencephalographic activity, neocortical neurons are bombarded continuously by correlated synaptic inputs at high frequency, which significantly affect their integrative properties. A series of predictions are suggested to test this model.

## INTRODUCTION

Since the classical view of passive dendritic integration was proposed for motoneurons 30 years ago (Fatt 1957), the intro-

The costs of publication of this article were defrayed in part by the payment of page charges. The article must therefore be hereby marked "advertisement" in accordance with 18 U.S.C. Section 1734 solely to indicate this fact.

duction of new experimental techniques such as intradendritic recordings (Linás and Nicholson 1971; Wong et al. 1979), and visually guided patch-clamp recording (Stuart et al. 1993; Yuste and Tank 1996) has revolutionized this area. These new approaches revealed that the dendrites of pyramidal neurons are involved actively in the integration of excitatory postsynaptic potentials (EPSPs) and that the activation of few synapses has powerful effects at the soma in brain slices (Markram et al. 1997; Mason et al. 1991; Thomson and Deuchars 1997). Although remarkably precise data have been obtained in slices, little is known about the integrative properties of the same neurons in vivo.

The synaptic connectivity of the neocortex is very dense. Each pyramidal cell receives 5,000–60,000 synapses (Cragg 1967; DeFelipe and Fariñas 1992), 70% of which originate from other cortical neurons (Gruner et al. 1974; Szentagothai 1965). Given that neocortical neurons spontaneously fire at 5–20 Hz in awake animals (Evarts 1964; Hubel 1959; Steriade 1978), cortical cells must experience tremendous synaptic currents that may have a significant influence on their integrative properties. This theme was explored by several modeling studies (Barrett 1975; Bernander et al. 1991; Holmes and Woody 1989), where it was predicted that synaptic activity may have a profound impact on dendritic integration. However, despite its possible importance for understanding neuronal function, the conductance due to synaptic activity was never measured in awake animals because of the paramount technical difficulties related to intracellular recordings in conscious animals.

To circumvent these difficulties, we constrained computational models of neocortical pyramidal neurons with in vivo intracellular data obtained in ketamine-xylazine-anesthetized cats before and after local perfusion of tetrodotoxin (TTX) (Paré et al. 1998b). The interest of this approach derives from the fact that under ketamine-xylazine anesthesia, cortical neurons oscillate ( $<1$  Hz) between two states, one where the network is quiescent and another where it displays a pattern of activity similar to the waking state (Steriade et al. 1993a,b) (Fig. 1A and B). Indeed, during these active periods (Fig. 1B, underlined epochs), as in the waking state (Fig. 1A), the electroencephalogram (EEG) is dominated by waves of low amplitude and high frequencies (20–60 Hz) and neocortical pyramidal neurons fire spontaneously at 5–20 Hz. Moreover, electrical stimulation of brain stem activating systems that are believed to maintain the awake state in normal circumstances elicits periods of desynchronized EEG activity with similar characteristics under ketamine-xylazine anesthesia (Steriade et al. 1993a).

Thus we estimated the synaptic activity required to account

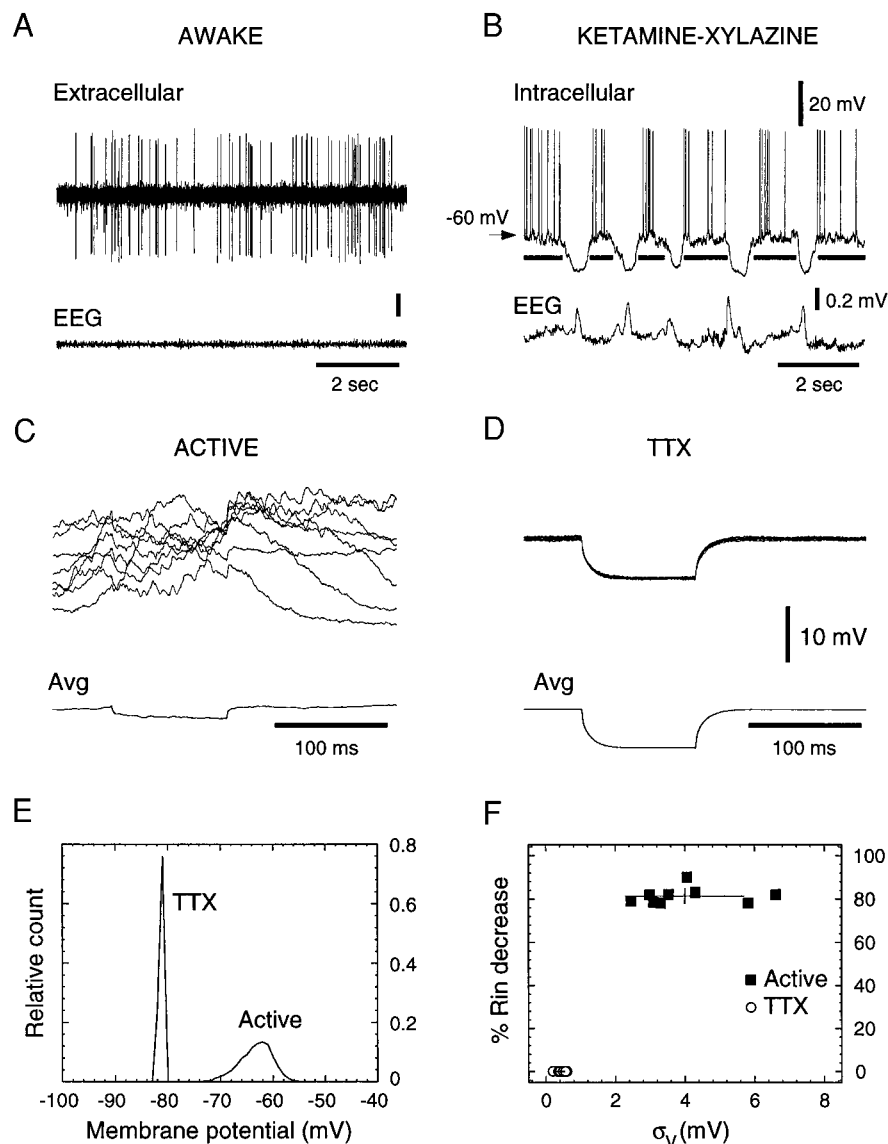


FIG. 1. Electrophysiological properties of neocortical pyramidal neurons during periods of intense synaptic activity. *A*: extracellularly recorded cortical neuron of the suprasylvian gyrus in an awake cat. This cell fired tonically at 7.1 Hz (Extracellular) while the electroencephalogram (EEG) displayed low-amplitude fast activity (20–60 Hz). *B*: intracellularly recorded cortical neuron of the same cortical area under ketamine-xylazine anesthesia using a K-acetate-filled pipette. “Active” periods (bars) alternate with deep hyperpolarizations. During active periods, this cortical neuron fired at  $\sim 7.3$  Hz while the EEG showed low-amplitude fast activities. *C*: low  $R_{in}$  during active periods. *Top*: during active periods, the voltage responses to intracellularly injected current pulses ( $-0.1$  nA) were highly variable (cell maintained hyperpolarized just below firing threshold). *Avg*: average of 50 pulses. *D*: same cell and current pulse amplitude as in *C* after application of TTX. *Top*: TTX suppressed most spontaneous events and produced a marked increase in  $R_{in}$  and time constant. *Avg*: average of 20 pulses. *E*:  $V_m$  distribution before and after TTX. During active periods (Active),  $V_m$  values were distributed between  $-70$  and  $-55$  mV, and the standard deviation was high ( $\sigma_v = 3.5$  mV in this case). TTX produced a marked hyperpolarization (to around  $-80$  mV) and a drop of  $\sigma_v$  (to  $\sim 0.4$  mV). *F*: graph plotting the percentage decrease in  $R_{in}$  (normalized to the  $R_{in}$  under TTX) as a function of  $\sigma_v$  for several cells during active periods and after TTX.

for the differences in neuronal properties observed *in vivo* during synaptic quiescence (i.e., in the presence of TTX) and during these active periods, here considered as a model of the spontaneous synaptic bombardment occurring in the waking state. The model then was used to infer the impact of this intense synaptic activity on dendritic integration.

## METHODS

### Intracellular recordings *in vivo*

We reanalyzed intracellular data obtained from neocortical pyramidal cells recorded in a previous study (Paré et al. 1998b). Unpublished intracellular recordings obtained with K-acetate-filled pipettes ( $n = 2$ ) also were included in the analysis. Briefly, intracellular recordings were obtained from morphologically identified neocortical pyramidal cells in the suprasylvian gyrus (area 5–7) of cats deeply anesthetized with a ketamine-xylazine mixture (11 and 2 mg/kg im), paralyzed with gallamine triethiodide, and artificially ventilated. The level of anesthesia was determined by continuously monitoring the EEG, and supplemental doses of ketamine-xylazine (2 and 0.3 mg/kg, respectively, iv) were given to maintain a synchronized EEG pattern.

Lidocaine (2%) was applied to all skin incisions. End-tidal  $CO_2$  concentration was kept at  $3.7 \pm 0.2\%$  (mean  $\pm$  SE) and the body temperature was maintained at  $37^\circ C$  with a heating pad. To ensure recording stability, the cisterna magna was drained, the cat was suspended, and a bilateral pneumothorax was performed. Intracellular recording electrodes consisted of glass capillary tubes pulled to a tip diameter of  $\sim 0.5 \mu m$  ( $\sim 30 M\Omega$ ) and filled with K-acetate or KCl (2.5 M). Details about experimental procedures and cell identification were given previously (Paré et al. 1998a,b). Experiments were conducted in agreement with ethics guidelines of the Canadian Council on Animal Care.

### TTX microperfusion *in vivo*

An injection micro-pipette (75  $\mu m$  tip diameter) was inserted  $\sim 2$  mm rostral to the recording micropipette to a depth of 1.5 mm. A solution (Ringer or Ringer + TTX, 50  $\mu M$ ) was pumped continuously through the injection pipette (1–1.5  $\mu l/min$ ) for the duration of the recording session; the dialyzing solution was changed using a liquid switch system. The Ringer solution contained (in mM) 126 NaCl, 26  $NaHCO_3$ , 3 KCl, 1.2  $KH_2PO_4$ , 1.6  $MgSO_4$ , 2  $CaCl_2$ , 5 HEPES, and 15 glucose. The blockade of synaptic activity by TTX was evidenced by the disappearance of responses to electrical stimuli applied to the

cortex using tungsten microelectrodes inserted 2 mm caudal to the recording pipette (see Paré et al. 1997, 1998b for more details).

### Estimation of membrane parameters

Membrane potential ( $V_m$ ) distributions were computed from concatenated epochs of intense synaptic activity totaling  $\sim 1$  min. The signal was sampled at 5 kHz (for a total of  $\sim 300,000$  data points), and the positive phase of action potentials was deleted digitally. The values of these data points (usually 2) were replaced by that of points immediately preceding the action potentials. No attempt was made to delete spike afterpotentials because they were distorted by spontaneous synaptic events. The average  $V_m$  ( $\langle V_m \rangle$ ) and the standard deviation ( $\sigma_v$ ) were computed from such distributions.

### Geometry for computational models

Simulations of cat layer II–III, layer V, and layer VI neocortical pyramidal cells were based on cellular reconstructions obtained from two previous studies (Contreras et al. 1997; Douglas et al. 1991). The cellular geometries were incorporated into the NEURON simulation environment (Hines and Carnevale 1997). The dendritic surface was corrected for spines, assuming that spines represent  $\sim 45\%$  of the dendritic membrane area (DeFelipe and Fariñas 1992). Surface correction was made by rescaling  $C_m$  and conductances by 1.45 as described previously (Bush and Sejnowski 1993; Paré et al. 1998a). An axon was added, consisting in an initial segment of 20  $\mu\text{m}$  length and 1  $\mu\text{m}$  diam, followed by 10 segments of 100  $\mu\text{m}$  length and 0.5  $\mu\text{m}$  diam each.

### Passive properties

Passive properties were adjusted to experimental recordings in the absence of synaptic activity: to block synaptic events mediated by glutamate  $\alpha$ -amino-3-hydroxy-5-methyl-4-isoxazolepropionic acid (AMPA) and  $\gamma$ -aminobutyric acid type-A (GABA<sub>A</sub>) receptors, the microperfusion solution contained: Ringer + TTX (50  $\mu\text{M}$ ) + 1,2,3,4-tetrahydro-6-nitro-2,3-dioxo-benzo[f]quinoxaline-7-sulfonamide disodium (NBQX, 200  $\mu\text{M}$ ) + bicuculline (200  $\mu\text{M}$ ). This procedure suppresses all miniature synaptic events, as demonstrated in a previous study (Paré et al. 1997).

Fitting of the model to passive responses obtained in such conditions of absence of synaptic activity was performed using a simplex algorithm (Press et al. 1986). Fitted parameters were leak conductance and reversal potential, whereas other passive parameters were fixed (membrane capacitance of 1  $\mu\text{F}/\text{cm}^2$  and axial resistivity of 250  $\Omega\text{cm}$ ). Other combinations of passive parameters were also considered, including a supplementary leak in the soma (10 nS) due to electrode impalement, combined with a lower leak conductance of 0.015  $\text{mS cm}^{-2}$  (Pongracz et al. 1991; Spruston and Johnston 1992) and/or a lower axial resistivity of 100  $\Omega\text{cm}$ .

In some simulations, a nonuniform distribution of leak parameters was used based on estimations in layer V neocortical pyramidal cells (Stuart and Spruston 1998). As estimated by these authors, the axial resistance was low (80  $\Omega\text{cm}$ ) and the leak conductance was low ( $g_{\text{leak}} = 0.019 \text{ mS cm}^{-2}$ ) in soma but high ( $g_{\text{leak}} = 0.125 \text{ mS cm}^{-2}$ ) in distal dendrites.  $g_{\text{leak}}$  was given by a sigmoid distribution  $1/g_{\text{leak}} = 8 + 44/\{1 + \exp[(x - 406)/50]\}$  where  $x$  is the distance to soma. The exact form of this distribution was obtained by fitting the model to passive responses as described above.

### Synaptic inputs

The densities of synapses in different regions of the cell were estimated from morphological studies of neocortical pyramidal cells (DeFelipe and Fariñas 1992; Fariñas and DeFelipe 1991a,b; Larkman 1991; Mungai 1967; White 1989). These densities (per 100  $\mu\text{m}^2$  of

membrane) were as follows: 10–20 GABAergic synapses in soma, 40–80 GABAergic synapses in axon initial segment, 8–12 GABAergic synapses, and 55–65 glutamatergic (AMPA) synapses in dendrites.

The kinetics of AMPA and GABA<sub>A</sub> receptor types were simulated using two-state kinetic models (Destexhe et al. 1994)

$$I_{\text{syn}} = \bar{g}_{\text{syn}} m (V - E_{\text{syn}}) \quad (1)$$

$$\frac{dm}{dt} = \alpha [T] (1 - m) - \beta m \quad (2)$$

where  $I_{\text{syn}}$  is the postsynaptic current,  $\bar{g}_{\text{syn}}$  is the maximal conductance,  $m$  is the fraction of open receptors,  $E_{\text{syn}}$  is the reversal potential,  $[T]$  is the transmitter concentration in the cleft, and  $\alpha$  and  $\beta$  are forward and backward binding rate constants of  $T$  to open the receptors.  $E_{\text{syn}} = 0 \text{ mV}$ ,  $\alpha = 1.1 \times 10^6 \text{ M}^{-1}\text{s}^{-1}$ ,  $\beta = 670 \text{ s}^{-1}$  for AMPA receptors;  $E_{\text{syn}} = -80 \text{ mV}$ ,  $\alpha = 5 \times 10^6 \text{ M}^{-1}\text{s}^{-1}$ ,  $\beta = 180 \text{ s}^{-1}$  for GABA<sub>A</sub> receptors. When a spike occurred in the presynaptic compartment, a pulse of transmitter was triggered such that  $[T] = 1 \text{ mM}$  during 1 ms. The kinetic parameters were obtained by fitting the model to postsynaptic currents recorded experimentally (see Destexhe et al. 1998). *N*-methyl-D-aspartate (NMDA) receptors are blocked by ketamine and were not included.

### Correlation of release events

In some simulations,  $N$  Poisson-distributed random presynaptic trains of action potentials were generated according to a correlation coefficient  $c$ . The correlation applied to any pair of presynaptic train, irrespective of the proximity of synapses on the dendritic tree and correlations were treated independently for excitatory and inhibitory synapses for simplicity. To generate correlated presynaptic trains, a set of  $N_2$  independent Poisson-distributed random variables was generated and distributed randomly among the  $N$  presynaptic trains. This procedure was repeated at every integration step such that the  $N_2$  random variables were redistributed constantly among the  $N$  presynaptic trains. Correlations arose from the fact that  $N_2 \leq N$  and the ensuing redundancy within the  $N$  presynaptic trains.  $N_2$  was chosen such as to generate a correlation of  $c = 0.05$ – $0.2$  calculated from the peak of the cross-correlation function. Typically,  $n = 16563$  and  $N_2 = 400$  gave a correlation value of  $c \sim 0.1$ .

### Active currents

Active currents were inserted into the soma, dendrites, and axon with different densities in accordance with available experimental evidence in neocortical and hippocampal pyramidal neurons (Hoffman et al. 1997; Magee and Johnston 1995; Magee et al. 1998; Stuart and Sakmann 1994). Active currents were expressed by the generic form

$$I_i = \bar{g}_i m^M h^N (V - E_i)$$

where  $\bar{g}_i$  is the maximal conductance of current  $I_i$  and  $E_i$  is its reversal potential. The current activates according to  $M$  activation gates, represented by the gating variable  $m$ . It inactivates with  $N$  inactivation gates represented by the gating variable  $h$ .  $m$  and  $h$  obey to first-order kinetic equations.

The voltage-dependent  $\text{Na}^+$  current was described by (Traub and Miles 1991)

$$I_{\text{Na}} = \bar{g}_{\text{Na}} m^3 h (V - E_{\text{Na}})$$

$$\frac{dm}{dt} = \alpha_m(V)(1 - m) - \beta_m(V)m$$

$$\frac{dh}{dt} = \alpha_h(V)(1 - h) - \beta_h(V)h$$

$$\alpha_m = \frac{-0.32(V - V_T - 13)}{\exp[-(V - V_T - 13)/4] - 1}$$

$$\beta_m = \frac{0.28(V - V_T - 40)}{\exp[(V - V_T - 40)/5] - 1}$$

$$\alpha_h = 0.128 \exp[-(V - V_T - V_S - 17)/18]$$

$$\beta_h = \frac{4}{1 + \exp[-(V - V_T - V_S - 40)/5]}$$

where  $V_T = -58$  mV was adjusted to obtain a threshold of around  $-55$  mV as in our experiments, and the inactivation was shifted by 10 mV toward hyperpolarized values ( $V_S = -10$  mV) to match the voltage dependence of  $\text{Na}^+$  currents in neocortical pyramidal cells (Huguenard et al. 1988). The pattern and kinetics of  $\text{Na}^+$  channels was similar to a previous study on hippocampal pyramidal cells (Hoffman et al. 1997): the density was low in soma and dendrites ( $120$  pS/ $\mu\text{m}^2$ ) and was 10 times higher in the axon.

The “delayed-rectifier”  $\text{K}^+$  current was described by (Traub and Miles 1991)

$$I_{Kd} = \bar{g}_{Kd} n^4 (V - E_K)$$

$$\frac{dn}{dt} = \alpha_n(V) (1 - n) - \beta_n(V) n$$

$$\alpha_n = \frac{-0.032(V - V_T - 15)}{\exp[-(V - V_T - 15)/5] - 1}$$

$$\beta_n = 0.5 \exp[-(V - V_T - 10)/40]$$

$\text{K}^+$  channel densities were of  $100$  pS/ $\mu\text{m}^2$  in soma and dendrites, and  $1,000$  pS/ $\mu\text{m}^2$  in the axon.

A noninactivating  $\text{K}^+$  current was described by (Mainen et al. 1995)

$$I_M = \bar{g}_M n (V - E_K)$$

$$\frac{dn}{dt} = \alpha_n(V) (1 - n) - \beta_n(V) n$$

$$\alpha_n = \frac{0.0001(V + 30)}{1 - \exp[-(V + 30)/9]}$$

$$\beta_n = \frac{-0.0001(V + 30)}{1 - \exp[(V + 30)/9]}$$

This current was present in soma and dendrites (density of  $2\text{--}5$  pS/ $\mu\text{m}^2$ ) and was responsible for spike frequency adaptation, as detailed previously (Paré et al. 1998a).

It was reported that some pyramidal cell have a hyperpolarization-activated current termed  $I_h$  (Spain et al. 1987; Stuart and Spruston 1998). However, most cells recorded in the present study had no apparent  $I_h$  (see passive responses in Figs. 1 and 2). Occasionally, cells displayed a pronounced  $I_h$ , but these cells were not included in the present study. This current was therefore not included in the model.

All simulations were done using NEURON (Hines and Carnevale 1997) on a Sparc-20 work-station (Sun Microsystems, Mountain View, CA).

## RESULTS

### Membrane properties of neocortical pyramidal neurons during active periods

In a previous study (Paré et al. 1998b), the properties of pyramidal neurons were compared before and after local TTX

application, revealing that differences in background synaptic activity account for much of the discrepancies between in vivo and in vitro recordings. Intracellular recordings were performed under barbiturate and ketamine-xylazine anesthesia, and the input resistance ( $R_{in}$ ) was estimated before and after TTX application (Paré et al. 1998b). However, these properties were never measured specifically during active periods. Here, we have reexamined and quantified these data by focusing specifically on active periods occurring under ketamine-xylazine anesthesia (Fig. 1B, bars). These active periods were identified as follows: neurons fire at  $\sim 5\text{--}20$  Hz, their membrane potential ( $V_m$ ) is around  $-65$  to  $-60$  mV, and the EEG displays low-amplitude waves of fast frequency in the gamma range. Active periods usually lasted  $\sim 0.4\text{--}2$  s, although periods lasting up to several seconds occasionally occurred (Steriade et al. 1993a).

During active periods, neocortical neurons had a low  $R_{in}$ , as shown by the relatively small voltage responses to intracellular current injection (Fig. 1C, top). Averaging  $>50$  pulses during active periods led to  $R_{in}$  of  $9.2 \pm 4.3$  M $\Omega$  ( $n = 26$ ), consistent with previous observations (Contreras et al. 1996).

The total conductance change due to synaptic activity was quantified by comparing the  $R_{in}$  of the cells during active periods to that measured after blocking synaptic transmission using microperfusion of TTX. Under TTX, injection of current pulses led to larger responses (Fig. 1D) and larger  $R_{in}$  values ( $46 \pm 8$  M $\Omega$ ;  $n = 9$ ). This was paralleled by a marked decrease in the amplitude of  $V_m$  fluctuations, as quantified by the standard deviation of the  $V_m$  ( $\sigma_v$ ; Fig. 1E). In nine different cells recorded successively during active periods and after TTX application,  $\sigma_v$  was reduced from  $4.0 \pm 2.0$  mV to  $0.4 \pm 0.1$  mV, respectively (Fig. 1F). Figure 1E also shows that the  $V_m$  dropped significantly to  $-80 \pm 2$  mV, as reported previously (Paré et al. 1998b). During active periods, the average  $V_m$  ( $\langle V_m \rangle$ ) was  $-65 \pm 2$  mV in control conditions (K-acetate-filled pipettes) and  $-51 \pm 2$  mV with chloride-filled recording pipettes. These conditions correspond to chloride reversal potentials ( $E_{Cl}$ ) of  $-73.8 \pm 1.6$  mV and  $-52.0 \pm 2.9$  mV, respectively (Paré et al. 1998a).

Normalizing  $R_{in}$  changes with reference to the  $R_{in}$  measured in the presence of TTX revealed that in all cells where active periods could be compared with an epoch of suppressed synaptic activity ( $n = 9$ ), the  $R_{in}$  was reduced by approximately the same relative amount ( $81.4 \pm 3.6\%$ ; Fig. 1F; data summarized in Table 1), independently of absolute values. Similar values were obtained by repeating this analysis at different  $V_m$ s, either more depolarized, by using chloride-filled pipettes ( $n = 7$ ), or more hyperpolarized, by steady current injection ( $-1$  nA;  $n = 2$ ). Taken together, these data show that active periods are characterized by an about fivefold decrease in  $R_{in}$ , a significant depolarization of  $15\text{--}30$  mV depending on the recording conditions, and a  $\sim 10$ -fold increase in the amplitude of  $V_m$  fluctuations.

### Model of high-frequency release

Computational models of cat neocortical pyramidal cells were used to estimate the release conditions and conductances necessary to account for these experimental measurements. A layer VI neocortical pyramidal cell (Fig. 2A) was reconstructed and incorporated in simulations (see METHODS). As both so-

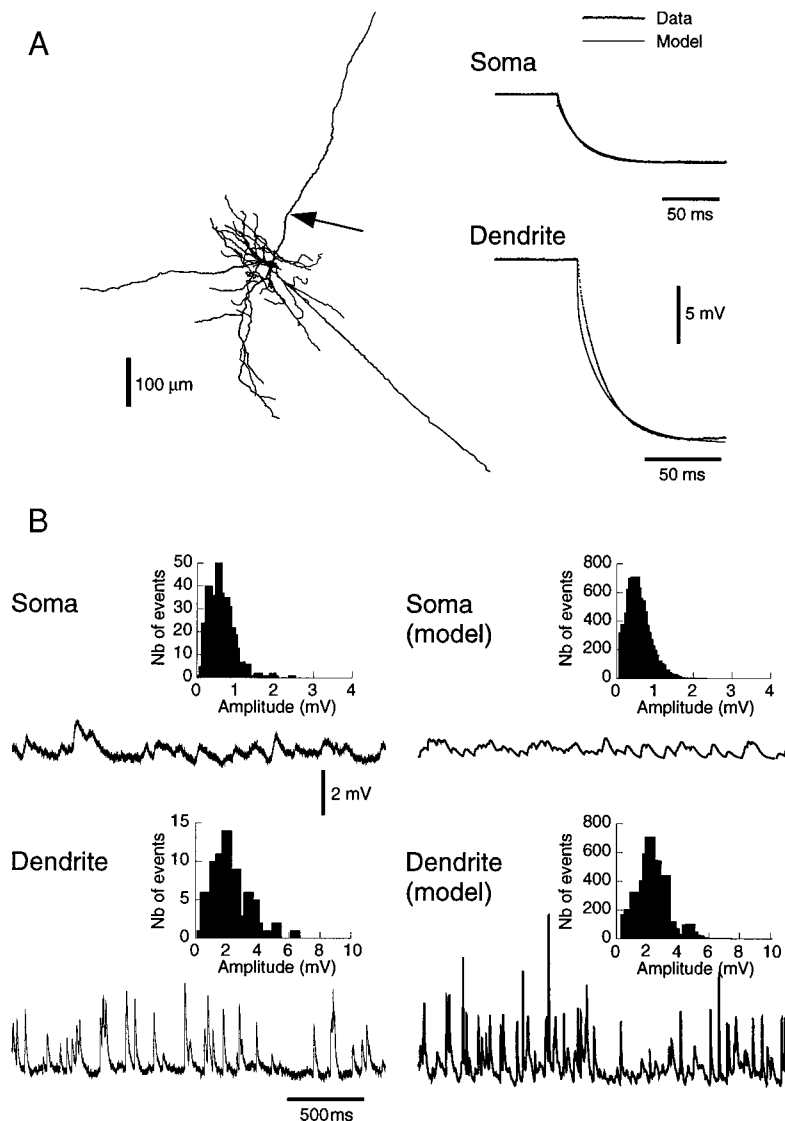


FIG. 2. Calibration of the model to passive responses and miniature synaptic events recorded intracellularly in vivo. *A*: morphology of a layer VI neocortical pyramidal cell from cat cerebral cortex, which was reconstructed and incorporated into computational models. Passive responses of the model were adjusted to somatic (Soma;  $-0.1$  nA current pulse) and dendritic recordings (Dendrite;  $-0.2$  nA current pulse) obtained in vivo in the presence of TTX and synaptic blockers (see METHODS). *B*: miniature synaptic potentials in neocortical pyramidal neurons. *Left*: TTX-resistant miniature events in somatic (Soma) and dendritic (Dendrite) recordings. Histograms of mini amplitudes are shown in the insets. *Right*: simulated miniature events; 16,563 glutamatergic and 3,376 GABAergic synapses were simulated with Poisson-distributed spontaneous release. Quantal conductances and release frequency were estimated by matching simulations to experimental data. Best fits were obtained with an average release frequency of 0.01 Hz and conductances of 1,200 and 600 pS at glutamatergic and GABAergic synapses, respectively.

matic and dendritic recordings are critical to constrain, the simulations of synaptic activity (see following text), passive responses from both types of recordings (Paré et al. 1997) were used to constrain the passive parameters of the model. The fitting was performed such that the same model could fit both somatic and dendritic recordings obtained in deep pyramidal cells in the absence of synaptic activity (TTX + synaptic blockers; see METHODS). The same model could fit both traces (Fig. 2A) with the following optimal passive parameters:  $g_{\text{leak}} = 0.045$  mS  $\text{cm}^{-2}$ ,  $C_m = 1$   $\mu\text{F}/\text{cm}^2$ , and  $R_i = 250$   $\Omega\text{cm}$  (see METHODS). Another fit was performed by forcing  $R_i$  to 100  $\Omega\text{cm}$  ( $C_m = 1$   $\mu\text{F}/\text{cm}^2$  and  $g_{\text{leak}} = 0.039$  mS  $\text{cm}^{-2}$ ). Although the latter set of values were not optimal, they were used to check for the dependence of the results on axial resistance. A passive fit also was performed with high membrane resistance, based on whole cell recordings (Pongracz et al. 1991; Spruston and Johnston 1992), and a somatic shunt due to electrode impalement. In this case, the parameters were as follows: 10 nS somatic shunt,  $g_{\text{leak}} = 0.0155$  mS  $\text{cm}^{-2}$ ,  $C_m = 1$   $\mu\text{F}/\text{cm}^2$ , and  $R_i$  was of either 250 or 100  $\Omega\text{cm}$ . A nonuniform leak conductance, low in soma and a high in distal dendrites (Stuart and

Spruston 1998), also was tested (see METHODS). No further effort was made to optimize passive parameters as models and experiments were based on different cellular morphologies. This fitting procedure ensured that the model had an  $R_{\text{in}}$  and a time constant consistent with both somatic and dendritic recordings free of synaptic activity.

The next step was to simulate TTX-resistant miniature synaptic potentials occurring in the same neurons. These miniature events were characterized in somatic and dendritic intracellular recordings after microperfusion of TTX in vivo (Paré et al. 1997) (Fig. 2B, left). To simulate them, a plausible range of parameters was determined based on in vivo experimental constraints. Then, a search within this parameter range was performed to find an optimal set that was consistent with all constraints. These constraints were the densities of synapses in different regions of the cell, as derived from morphological studies of neocortical pyramidal cells (DeFelipe and Fariñas 1992; Fariñas and DeFelipe 1991a,b; Larkman 1991; Mungai 1967; White 1989) (see METHODS); the quantal conductance at AMPA and GABA<sub>A</sub> synapses, as determined by whole cell recordings of neocortical neurons (Markram et al. 1997; Salin

TABLE 1. *Membrane parameters of neocortical neurons during intense synaptic activity and after TTX*

Parameter Measured	Experiments	Model	
		Passive	$I_{Na^+}$ , $I_{Kd}$ , $I_M$
$\sigma_v$ , mV	$4.0 \pm 2.0$	3.6–4.0	3.8–4.2
$\langle V_m \rangle$ (KAc), mV	$-65 \pm 2$	-63.0 to -66.1	-64.3 to -66.4
$\langle V_m \rangle$ (KCl), mV	$-51 \pm 2$	-50.1 to -52.2	-50.7 to -53.1
$\sigma_v$ (TTX), mV	$0.4 \pm 0.1$	0.3–0.4	—
$\langle V_m \rangle$ (TTX), mV	$-80 \pm 2$	-80	—
$R_{in}$ change, %	$81.4 \pm 3.6$	79–81	80–84

Experimental values were measured in intracellularly recorded pyramidal neurons *in vivo* (Experiments). The average value ( $\langle V_m \rangle$ ) and standard deviation ( $\sigma_v$ ) of the  $V_m$  are indicated, as well as the  $R_{in}$  change, during active periods and after TTX application. The values labeled “TTX” correspond to somatic recordings of miniature synaptic potentials. Experimental values are compared to the layer VI pyramidal cell model where active periods were simulated by correlated high-frequency release on glutamatergic and GABAergic receptors. The model is shown without voltage-dependent currents (passive; same model as in Fig. 3D4) and with voltage-dependent currents distributed in soma and dendrites ( $Na^+$  and  $K^+$  currents; same model as in Fig. 9A). The range of values indicate different combinations of release frequency (from 75 to 150% of optimal values). Miniature synaptic events were simulated by uncorrelated release events at low frequency (same model as in Fig. 2B). See text for more details.

and Prince 1996; Stern et al. 1992); the value of  $\sigma_v$  during miniature events after TTX application *in vivo* ( $\sim 0.4$  mV for somatic recordings and  $0.6$ – $1.6$  mV for dendritic recordings) (Paré et al. 1997); the change in  $R_{in}$  due to miniature events, as determined *in vivo* ( $\sim 8$ – $12\%$  in soma and  $30$ – $50\%$  in dendrites) (Paré et al. 1997); and the distribution of mini amplitudes and frequency, as obtained from *in vivo* somatic and dendritic recordings (Fig. 2B, insets).

An extensive search in this parameter range was performed and a narrow region was found to satisfy the above constraints. The optimal values found were a density of 20 GABAergic synapses per  $100 \mu m^2$  in the soma, 60 GABAergic synapses per  $100 \mu m^2$  in the initial segment, 10 GABAergic synapses and 60 glutamatergic (AMPA) synapses per  $100 \mu m^2$  in the dendrites; a rate of spontaneous release (assumed uniform for all synapses) of  $0.009$ – $0.012$  Hz; and quantal conductances of  $1,000$ – $1,500$  pS for glutamatergic and  $400$ – $800$  pS for GABAergic synapses. In these conditions, simulated miniature events were consistent with experiments (Fig. 2B, right), with  $\sigma_v$  of  $0.3$ – $0.4$  mV in soma and  $0.7$ – $1.4$  mV in dendrites, and  $R_{in}$  changes of  $8$ – $11\%$  in soma and  $25$ – $37\%$  in dendrites.

To simulate the intense synaptic activity occurring during active periods, we hypothesized that miniature events and active periods are generated by the same population of synapses with different conditions of release for GABAergic and glutamatergic synapses. The preceding model of miniature events was used to simulate active periods by increasing the release frequency at all synaptic terminals. Poisson-distributed release was simulated with identical release frequency for all excitatory synapses ( $f_e$ ) as well as for inhibitory synapses ( $f_i$ ). The release frequencies  $f_e$  and  $f_i$  affected the  $R_{in}$  and average  $V_m$  ( $\langle V_m \rangle$ ) (Fig. 3A). These aspects were constrained by the following experimental measurements (see preceding section): the  $R_{in}$  change produced by TTX should be  $\sim 80\%$ ; the  $V_m$  should be around  $-80$  mV without synaptic activity; the  $V_m$  should be about  $-65$  mV during active periods ( $E_{Cl} = -75$  mV); and the  $V_m$  should be around  $-51$  mV during active

periods recorded with chloride-filled electrodes ( $E_{Cl} = -55$  mV). Here again an extensive search in this parameter space was performed, and several combinations of excitatory and inhibitory release frequencies could reproduce correct values for the  $R_{in}$  decreases and  $V_m$  differences between active periods and after TTX (Fig. 3A). The optimal values of release frequencies were  $f_e = 1$  Hz (range  $0.5$ – $3$  Hz) for excitatory synapses and  $f_i = 5.5$  Hz (range  $4$ – $8$  Hz) for inhibitory synapses.

An additional constraint was the large  $V_m$  fluctuations experimentally observed during active periods, as quantified by  $\sigma_v$  (see preceding section). As shown in Fig. 3B ( $\square$ ,  $\circ$ ,  $\bullet$ ,  $\triangle$ ), increasing the release frequency of excitatory or inhibitory synapses produced the correct  $R_{in}$  change but always gave too small values of  $\sigma_v$ . High release frequencies led to membrane fluctuations of small amplitude, due to the large number of summing random events (Fig. 3B4). Variations within  $50$ – $200\%$  of the optimal value of different parameters, such as synapse densities, synaptic conductances, frequency of release, leak conductance, and axial resistance, could yield approximately correct  $R_{in}$  changes and correct  $V_m$  but failed to account for values of  $\sigma_v$  observed during active periods (Fig. 3C,  $\times$ ).

One additional assumption had to be made to reproduce  $V_m$  fluctuations comparable to those occurring *in vivo*. In the cortex, action potential-dependent release is clearly not independent at different synapses, as single axons usually establish several contacts in pyramidal cells (Markram et al. 1997; Thomson and Deuchars 1997). More importantly, the presence of oscillatory amplitude fluctuations in the EEG (see Fig. 1, A and B) implies correlated activity in the network. A correlation therefore was included in the release of different synapses (see METHODS). For the sake of simplicity, the correlation was irrespective of the proximity of synapses on the dendritic tree and correlations were treated independently for excitatory and inhibitory synapses. Figure 3D shows simulations of random synaptic bombardment similar to Fig. 3B4 but using different correlation coefficients. The horizontal alignment of the open symbols in Fig. 3D5 shows that the degree of correlation had a negligible effect on the  $R_{in}$  because the same amount of inputs occurred on average. However, the degree of correlation affected the standard deviation of the signal. Several combinations of excitatory and inhibitory correlations, within the range of  $0.05$ – $0.1$ , gave rise to  $V_m$  fluctuations with comparable  $\sigma_v$  as those observed experimentally during active periods (Fig. 3D5; compare with Fig. 1F; see also Table 1). Introducing correlations among excitatory or inhibitory inputs alone showed that excitatory correlations were most effective in reproducing the  $V_m$  fluctuations (Fig. 3D5,  $\triangle$ ).

To check if these results were affected by voltage-dependent currents, we estimated the voltage-dependent currents present in cortical cells from their current-voltage ( $I$ - $V$ ) relationship. The  $I$ - $V$  curve of a representative neocortical cell after TTX microperfusion is shown in Fig. 4A. The  $I$ - $V$  curve was approximately linear at  $V_m$ s more hyperpolarized than  $-60$  mV but displayed an important outward rectification at more depolarized potentials similar to *in vitro* observations (Stafstrom et al. 1982). The  $R_{in}$  was of  $\sim 57.3$  M $\Omega$  at values around rest (about  $-75$  mV) and  $30.3$  M $\Omega$  at more depolarized  $V_m$  (greater than  $-60$  mV), which represents a relative  $R_{in}$  change of  $47\%$ . This cell had the strongest outward rectification in six cells measured after TTX (relative  $R_{in}$  change of  $30 \pm 11\%$ ,  $n = 6$ ).

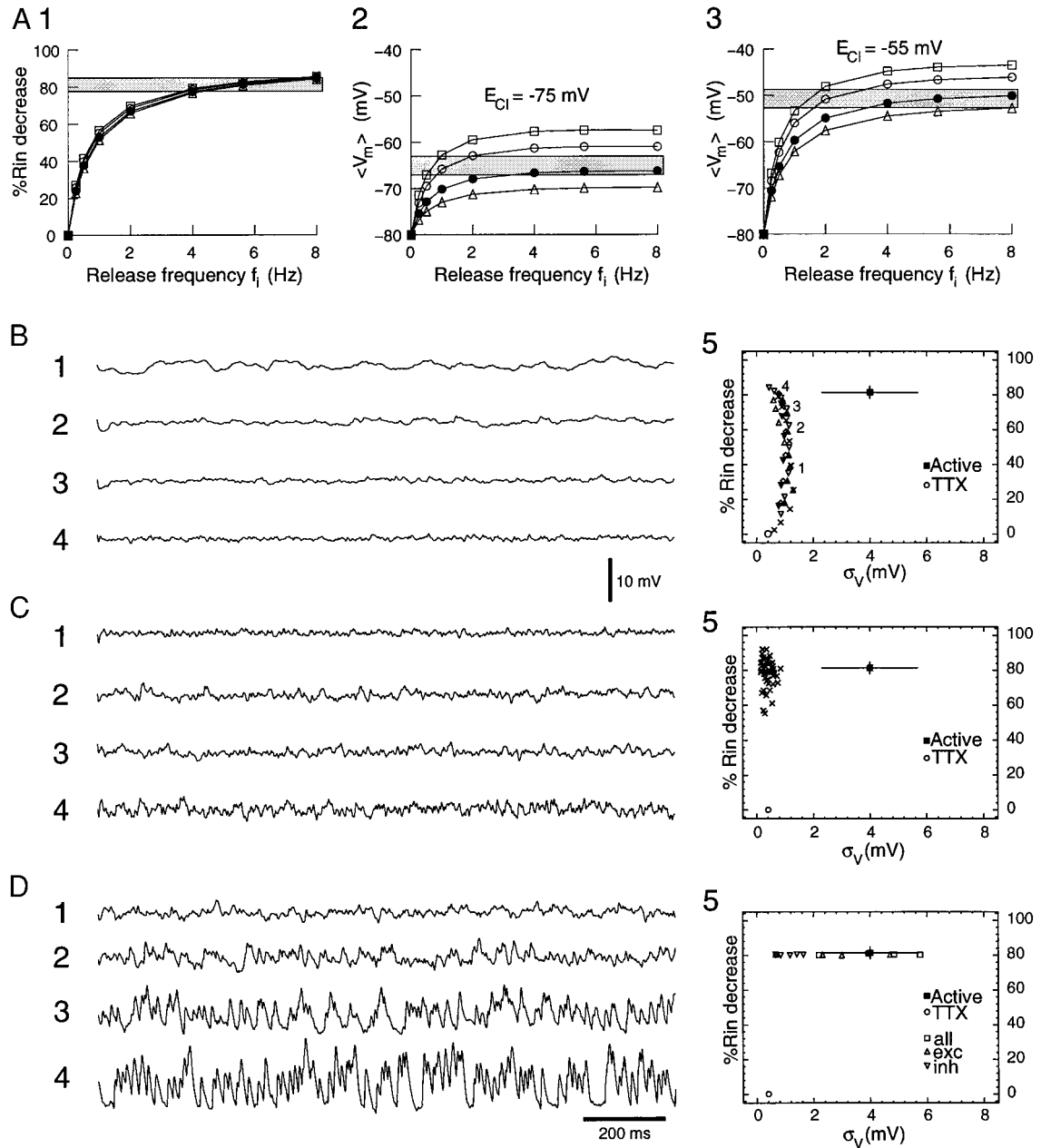


FIG. 3. Constraining the release parameters of the model to simulate periods of intense synaptic activity. *A*: effect of release frequencies on  $R_{in}$  (A1) and average  $V_m$  ( $\langle V_m \rangle$ ) for 2 values of chloride reversal potential  $E_{Cl}$  (A2 and A3). Both excitatory ( $f_e$ ) and inhibitory ( $f_i$ ) release frequencies were varied; each curve represents different ratios between them:  $f_e = 0.4 f_i$  ( $\square$ ),  $f_e = 0.3 f_i$  ( $\circ$ ),  $f_e = 0.18 f_i$  ( $\bullet$ ),  $f_e = 0.1 f_i$  ( $\triangle$ ).  $\blacksquare$ , range of values observed during in vivo experiments using either KAc- or KCl-filled pipettes. Optimal value was  $f_e = 1$  Hz and  $f_i = 5.5$  Hz. *B*: increasing the release frequency can account for the experimentally observed  $R_{in}$  decrease but not for the standard deviation of  $V_m$  ( $\sigma_v$ ). *B1–B4*: effect of increasing the release frequency up to  $f_e = 1$  Hz,  $f_i = 5.5$  Hz (*B4*). Different symbols in the graph (*B5*) indicate different combinations of release frequencies, synaptic conductances and densities. *C*: several combinations of conductance and release frequencies could yield correct  $R_{in}$  decrease but failed to reproduce  $\sigma_v$ . *C1–C4*: different parameter combinations giving the highest  $\sigma_v$ . All parameters were varied within 50–200% of their value in *B4* and are shown by crosses in *C5*. *D*: introducing a correlation between release events led to correct  $R_{in}$  and  $\sigma_v$ . *D1–D4*: these correspond to  $f_e = 1$  Hz and  $f_i = 5.5$  Hz, as in *B4*, with increasing values of correlation (0.025, 0.05, 0.075, and 0.1 from *D1* to *D4*). *D5*:  $\circ$ ,  $\square$ ,  $\triangle$ , and  $\nabla$ ,  $R_{in}$  and  $\sigma_v$  obtained with different values of correlation (between 0 and 0.2) when all inputs ( $\square$ ), only excitatory inputs ( $\triangle$ ) or only inhibitory inputs ( $\nabla$ ) were correlated.

In the model, this type of  $I$ - $V$  relation was simulated by including two voltage-dependent  $K^+$  currents,  $I_{Kd}$  and  $I_M$  (see METHODS). In the presence of these two currents, the model displayed a comparable rectification as the cell showing the strongest rectification in experiments under TTX (Fig. 4*B*; the straight lines indicate the same linear fits as in *A* for comparison).

The constraining procedure described above then was used to estimate the release conditions in the presence of voltage-dependent currents. First, the model including  $I_{Kd}$  and  $I_M$  was fit to passive traces obtained in the absence of synaptic activity to estimate the leak conductance and leak reversal (similar to Fig. 2*A*). Second, the release rate required to account for the  $\sigma_v$

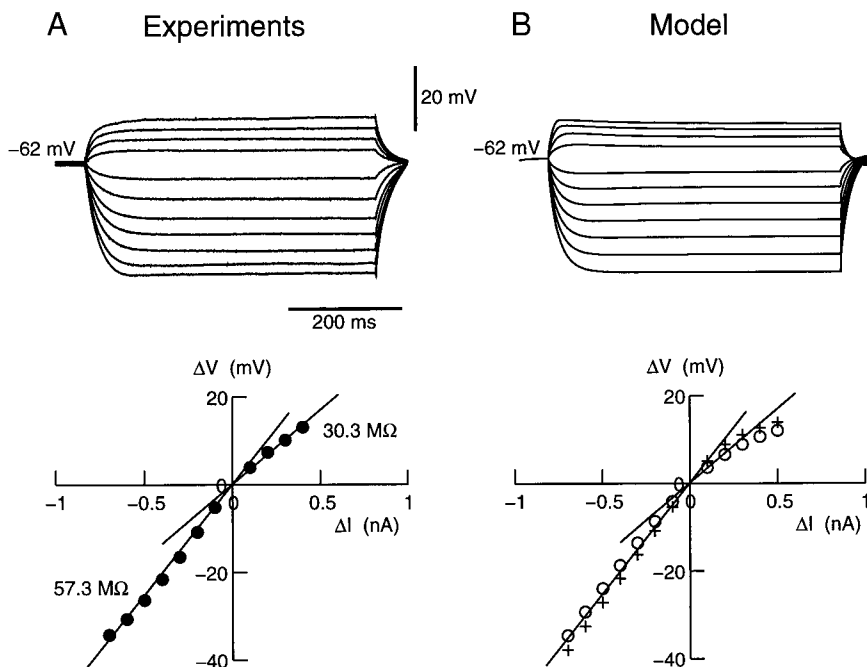


FIG. 4. Outward rectification of neocortical pyramidal neurons. *A*: current-voltage relation of a deep pyramidal neuron after microperfusion of TTX. This cell had a resting  $V_m$  of  $-75$  mV after TTX and was maintained at  $-62$  mV by DC current injection. Current-voltage ( $I$ - $V$ ) relation obtained by additional injection of current pulses of different amplitudes.  $I$ - $V$  relation revealed a significant reduction of  $R_{in}$  at depolarized levels (straight lines indicate the best linear fits). *B*: simulation of the same protocol in the model pyramidal neuron. Model had 2 voltage-dependent  $K^+$  currents,  $I_{Kd}$  ( $100$  pS/ $\mu m^2$ ) and  $I_M$  ( $2$  pS/ $\mu m^2$ ).  $I$ - $V$  relation obtained in the presence of both currents (circles) and compared with the same model with  $I_M$  removed (+). Model displayed a comparable rectification as experiments, although more pronounced (straight lines indicate the same linear fits as in *A* for comparison).

and  $R_{in}$  change produced by miniature events was estimated as in Fig. 2*B*. Third, we estimated the release rates that could best reproduce the  $R_{in}$ ,  $\langle V_m \rangle$  and  $\sigma_v$  (see Fig. 3).

The presence of voltage-dependent currents produced small—but detectable—changes in the optimal release conditions. For example, the same  $R_{in}$  change,  $\langle V_m \rangle$  and  $\sigma_v$  as the passive model with  $f_e = 1$  Hz and  $f_i = 5.5$  Hz was obtained with  $f_e = 0.92$  Hz and  $f_i = 5.0$  Hz (8–9% lower) in a model containing  $I_{Kd}$  and  $I_M$ . Both models gave nearly identical  $\sigma_v$  values for the same value of correlation. A similar constraining procedure also was performed using a nonuniform leak distribution with high leak conductances in distal dendrites (see METHODS), in addition to  $I_{Kd}$  and  $I_M$ , and nearly identical results were obtained (not shown). We therefore conclude that leak and voltage-dependent  $K^+$  currents have a small contribution to the  $R_{in}$  and  $\sigma_v$  of active periods, which are mostly determined by synaptic activity.

#### Impact of synaptic activity on integrative properties

The experimental evidence for a  $\sim 80\%$  decrease in  $R_{in}$  due to synaptic bombardment betrays a massive opening of ion channels. In the model, the total conductance due to synaptic activity was 7–10 times larger than the leak conductance. In conditions of high membrane resistance based on whole cell recordings (Pongracz et al. 1991; Spruston and Johnston 1992), the conductance due to synaptic activity was 20–30 times larger than the dendritic leak conductance.

The impact of this massive increase in conductance on dendritic attenuation was investigated by comparing the effect of current injection in active periods and synaptic quiescence (Fig. 5). In the absence of synaptic activity (Fig. 5*B*, smooth traces), somatic current injection (Fig. 5*B*, left) elicited large voltage responses in dendrites, and reciprocally (Fig. 5*B*, right), showing a moderate electrotonic attenuation. By contrast, during simulated active periods (Fig. 5*B*, noisy traces), voltage responses to identical current injections were reduced

markedly, betraying a greatly enhanced electrotonic attenuation. In these conditions, the relative amplitude of the deflection induced by the same amount of current with and without synaptic activity, as well as the difference in time constant, were in agreement with experimental observations (compare Fig. 5*B*, Soma, with Fig. 1, *C* and *D*). The effect of synaptic bombardment on the time constant was also in agreement with previous models (Bernander et al. 1991; Holmes and Woody 1989; Koch et al. 1996).

Dendritic attenuation was characterized further by computing somatodendritic profiles of  $V_m$  with steady current injection in the soma: in the absence of synaptic activity (Fig. 5*C*, Quiet), the decay of  $V_m$  after somatic current injection was characterized by space constants of 515–930  $\mu m$ , depending on the dendritic branch considered, whereas the space constant was reduced by about fivefold (105–181  $\mu m$ ) during simulated active periods (Fig. 5*C*, Active).

To estimate the convergence of synaptic inputs necessary to evoke a significant somatic depolarization during active periods, a constant density of excitatory synapses was stimulated synchronously in “proximal” and “distal” regions of dendrites (as indicated in Fig. 6*A*). In the absence of synaptic activity, simulated EPSPs had large amplitudes (12.6 mV for proximal and 6.0 mV for distal; Fig. 6*B*, Quiet). By contrast, during simulated active periods, the same stimuli gave rise to EPSPs that were barely distinguishable from spontaneous  $V_m$  fluctuations (Fig. 6*B*, Active). The average EPSP amplitude was 5.4 mV for proximal and 1.16 mV for distal stimuli (Fig. 6*B*, Active, avg), showing that EPSPs are attenuated by a factor of 2.3–5.2 in this case, with the maximal attenuation occurring for distal EPSPs. Figure 6*C* shows the effect of increasing the number of synchronously activated synapses. In quiescent conditions,  $< 50$  synapses on basal dendrites were sufficient to evoke a 10-mV depolarization at the soma (Quiet, proximal), and the activation of  $\sim 100$  distal synapses was needed to achieve a similar depolarization (Quiet, distal). During simulated active periods,  $> 100$  basal dendritic synapses were nec-

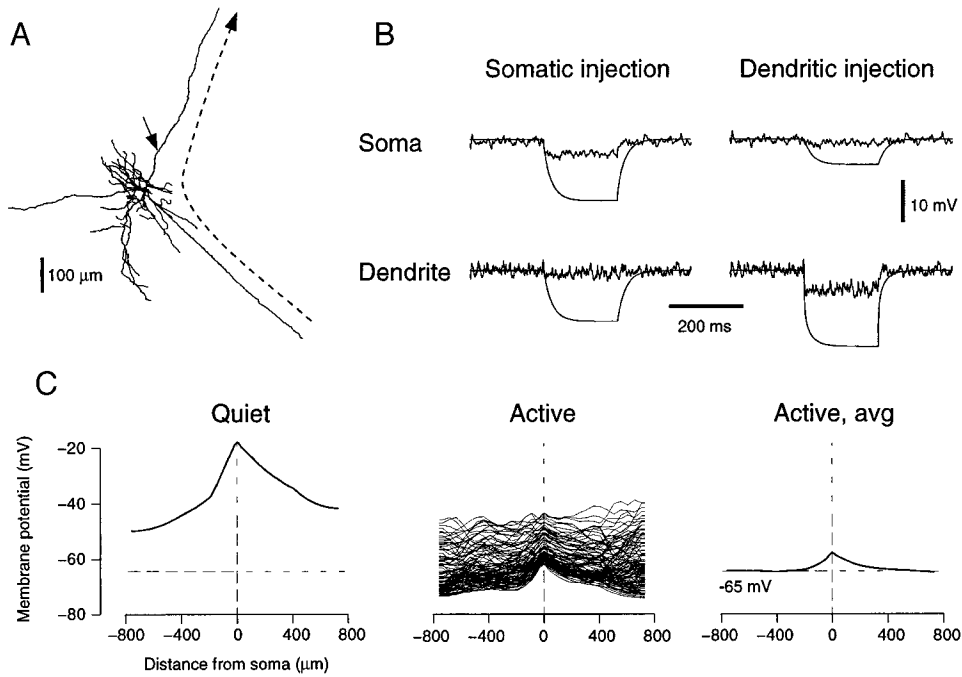


FIG. 5. Passive dendritic attenuation during simulated active periods. *A*: layer VI pyramidal cell used for simulations. *B*: injection of hyperpolarizing current pulses in the soma (left,  $-0.1$  nA) and a dendritic branch (right,  $-0.25$  nA). Dendritic voltage is shown at the same site as the current injection (indicated by a small arrow in *A*). Activity during simulated active periods (noisy traces; average of 50 pulses) is compared with the same simulation in the absence of synaptic activity (smooth lines). *C*: somato-dendritic  $V_m$  profile along the path indicated by a dashed line in *A*.  $V_m$  profile is shown at steady state after injection of current in the soma ( $+0.8$  nA). In the absence of synaptic activity (Quiet), there was moderate attenuation. During simulated active periods (Active), the profile was fluctuating (100 traces shown) but the average of 1,000 sweeps (Active, avg) revealed a marked attenuation of the steady-state voltage.

essary to reliably evoke a 10-mV somatic depolarization (Active, proximal), whereas the synchronous excitation of  $\leq 415$  distal synapses only evoked depolarization of a few millivolts (Active, distal).

To determine whether these results are dependent on the specific morphology of the studied cell, four different cellular geometries were compared, ranging from small layer II–III cells to large layer V pyramidal cells (Fig. 7*A*). In experiments,

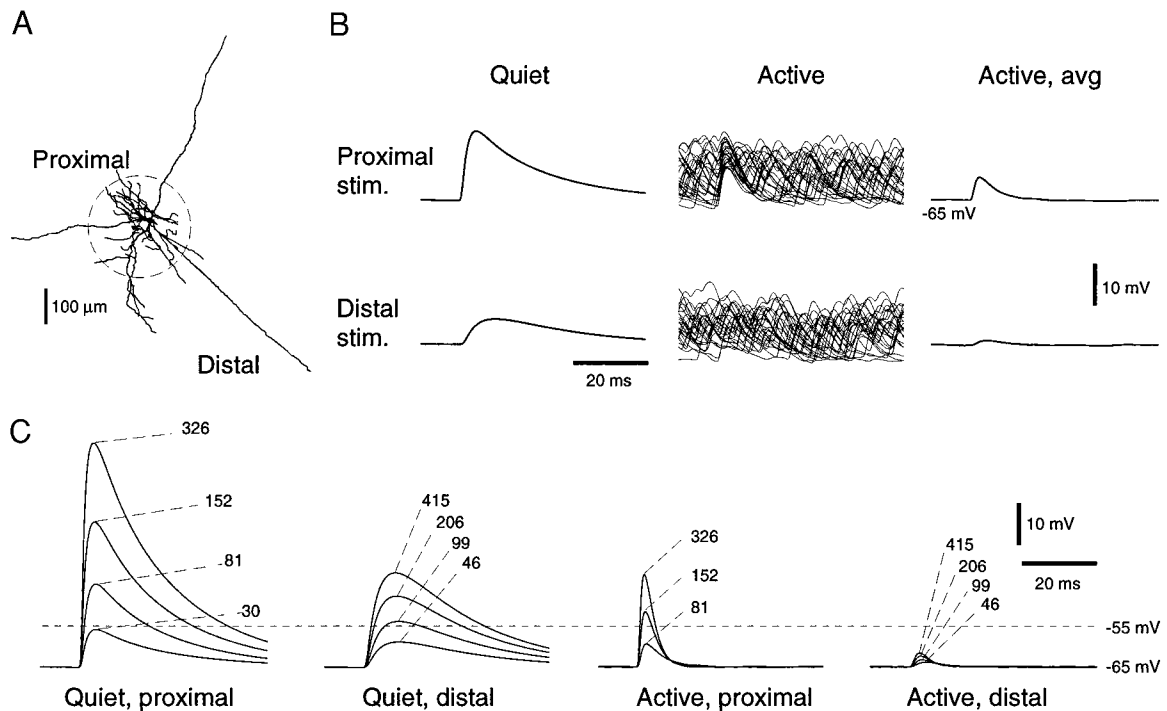


FIG. 6. Somatic depolarization necessitates the convergence of a large number of excitatory inputs during simulated active periods. *A*: layer VI pyramidal cell was divided into 2 dendritic regions: “Proximal” included all dendritic branches laying within  $200$   $\mu\text{m}$  from the soma (circle) and “Distal” referred to dendritic segments outside this region. *B*: attenuation after synchronized synaptic stimulation. Density of 1 excitatory synapse per  $200$   $\mu\text{m}^2$  was stimulated in proximal (81 synapses) and distal regions (46 synapses). Responses obtained in the absence of synaptic activity (Quiet) are compared with those observed during simulated active periods (Active; 25 traces shown). In the presence of synaptic activity (Active), the evoked EPSP was visible only when proximal synapses were stimulated. Average EPSPs (Active, avg;  $n = 1000$ ) showed a marked attenuation compared with the quiescent case. *C*: averaged EPSPs obtained with increasing numbers of synchronously activated synapses. Protocols similar to *B* were followed for different numbers of synchronously activated synapses (indicated for each trace). Horizontal dashed line indicates a typical value of action potential threshold.

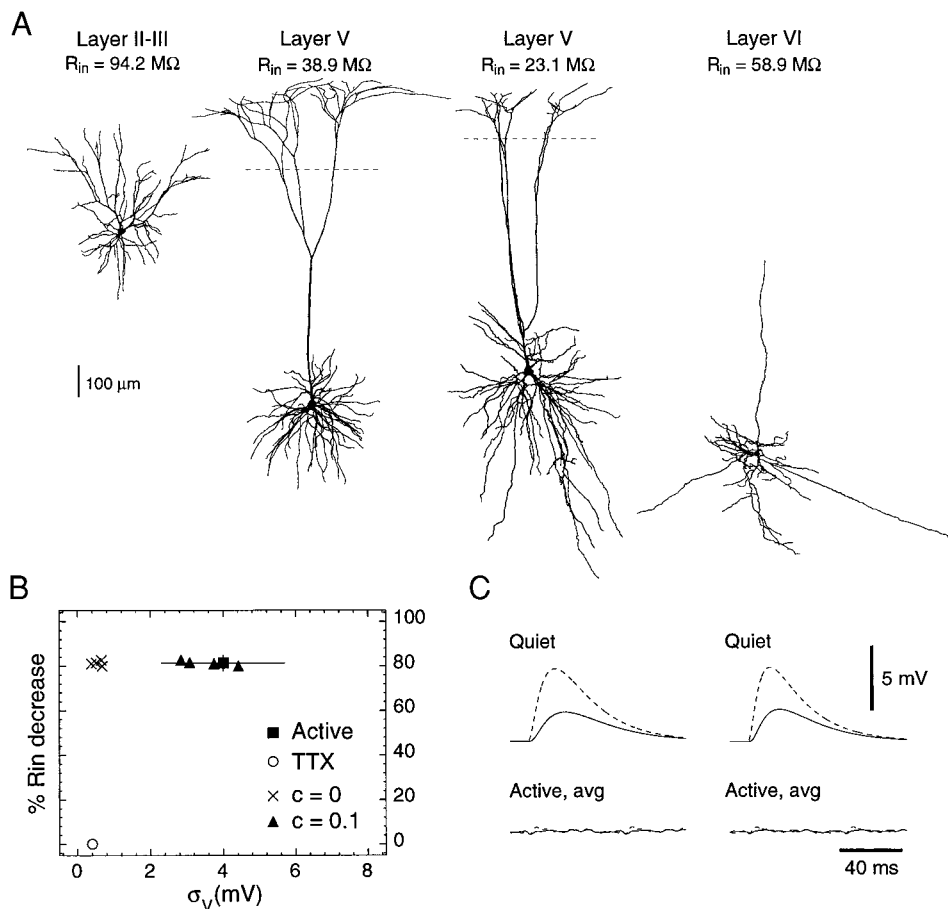


FIG. 7. Effect of dendritic morphology on membrane parameters during intense synaptic activity. *A*: 4 cellular reconstructions from cat neocortex used in simulations. All cells are shown at the same scale and their  $R_{in}$  was measured in the absence of synaptic activity (identical passive parameters for all cells). *B*: graph plotting the  $R_{in}$  decrease as a function of the standard deviation of the signal for these 4 cells. For all cells, the release frequency was the same ( $f_c = 1$  Hz,  $f_i = 5.5$  Hz). Results obtained without correlation ( $\times$ ) and with a correlation of  $c = 0.1$  ( $\blacktriangle$ ) are indicated. *C*: attenuation of distal EPSPs in 2 layer V cells. Excitatory synapses were stimulated synchronously in the distal apical dendrite ( $>800$   $\mu$ m from soma; indicated by dashed lines in *A*). EPSPs resulting from the stimulation of 857 (left) and 647 AMPA synapses (right, 23.1 M $\Omega$  cell) are shown for quiescent (Quiet) and active conditions (Active). These EPSPs were  $\sim 2$ – $3$  mV in amplitude without synaptic activity but were undetectable during active periods. Same simulation, performed with low axial resistance (100  $\Omega$ cm; dashed lines), gave qualitatively identical results.

the absolute  $R_{in}$  values varied from cell to cell. However, the relative  $R_{in}$  change produced by TTX was similar in all cells recorded. Similarly, in the model, the absolute  $R_{in}$  values depended on the cellular geometry: using identical passive parameters, the  $R_{in}$  values of the four neurons shown in Fig. 7A ranged from 23 to 94 M $\Omega$ . However, high-frequency release conditions had a similar impact on their membrane properties. Using identical synaptic densities, synaptic conductances, and release conditions as detailed above led to a decrease in  $R_{in}$  of  $\sim 80\%$  for all cells (Fig. 7B).  $V_m$  fluctuations also depended critically on the degree of correlation between the release of different synapses. Uncorrelated events produced too small  $\sigma_v$  (Fig. 7B,  $\times$ ), whereas a correlation of 0.1 could reproduce both the  $R_{in}$  change and  $\sigma_v$  (Fig. 7B,  $\blacktriangle$ ). The value of  $\sigma_v$  was correlated with cell size (not shown), and the variability of  $\sigma_v$  values was relatively high compared with that of  $R_{in}$  decreases. The effect of synaptic activity on dendritic attenuation was also independent of the cell geometry: the space constant was reduced by about fivefold in all four cells (not shown). Moreover, for the two layer V neurons, stimulating several hundreds of synapses at a distance of  $>800$   $\mu$ m from the soma had undetectable effects during active periods (Fig. 7C). This result was also reproduced using low axial resistivities (Fig. 7C, dashed lines).

These results show that intense synaptic activity has a drastic effect on the attenuation of distal synaptic inputs. However, voltage-dependent currents in dendrites may amplify EPSPs (Cook and Johnston 1997) or trigger dendritic spikes that propagate toward the soma (Stuart et al. 1997). Therefore the

attenuation of EPSPs must be reexamined in models that include active dendritic currents.

#### Firing properties during active periods

The response of the simulated neuron to depolarizing current pulses was tested in the presence of voltage-dependent  $\text{Na}^+$  currents, in addition to  $I_{Kd}$  and  $I_M$ . In the absence of synaptic activity (Fig. 8A), the model displayed pronounced spike frequency adaptation due to  $I_M$ , similar to “regular spiking” pyramidal cells in vitro (Connors et al. 1982). However, spike frequency adaptation was not apparent in the presence of correlated synaptic activity (Fig. 8B), probably due to the very small conductance of  $I_M$  compared with synaptic conductances. Nevertheless, the presence of  $I_M$  affected the firing behavior of the cell, as suppressing this current enhanced the excitability of the cell (Fig. 8B, No  $I_M$ ). This is consistent with the increase of excitability demonstrated in neocortical slices (McCormick and Prince 1986) after suppression of  $I_M$  by application of acetylcholine.

In the presence of  $\text{Na}^+$  and  $\text{K}^+$  voltage-dependent currents, simulated active periods generated “spontaneous” firing at an average rate that depended on the action potential threshold, which was affected by  $\text{Na}^+$  current densities. Setting the threshold at about  $-55$  mV in soma, based on our experiments, led to a sustained firing rate of  $\sim 10$  Hz (Fig. 9A), with all other features consistent with the model described earlier. In particular, the  $R_{in}$  reductions and values

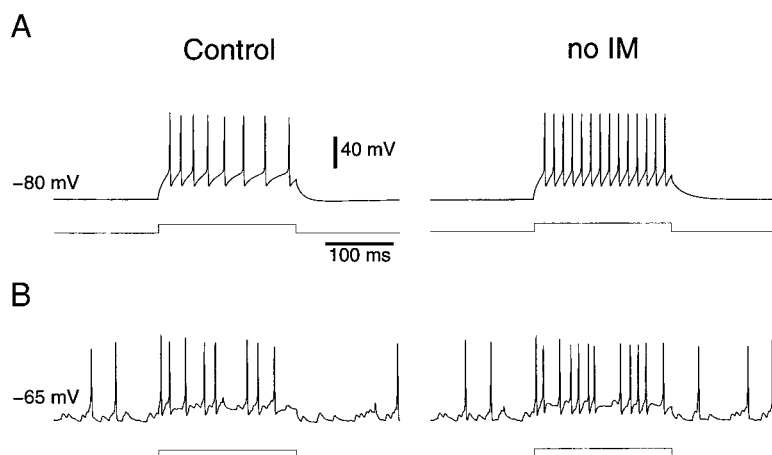


FIG. 8. Model of spike frequency adaptation with and without synaptic activity. *A*: in the absence of synaptic activity, the slow voltage-dependent  $K^+$  current  $I_M$  caused spike frequency adaptation in response to depolarizing current pulses (Control; 1 nA injected from resting  $V_m$  of  $-80$  mV). Same stimulus did not elicit spike frequency adaptation in the absence of  $I_M$  (No  $I_M$ ). *B*: in the presence of correlated synaptic activity, spike frequency adaptation was not apparent although the same  $I_M$  conductance was used (Control; depolarizing pulse of 1 nA from resting  $V_m$  of approximately equal to  $-65$  mV). Without  $I_M$ , the excitability of the cortical pyramidal cell was enhanced (No  $I_M$ ).

of  $\sigma_v$  produced by synaptic activity were affected minimally by the presence of voltage-dependent currents (Table 1). However, this was only valid for  $R_{in}$  calculated in the linear region of the  $I$ - $V$  relation (less than  $-60$  mV; see Fig. 4). Thus at  $V_m$ s more negative than  $-60$  mV, the membrane parameters are essentially determined by background synaptic currents with a minimal contribution from intrinsic voltage-dependent currents.

In these conditions, the firing rate of the cell was sensitive to the release frequency: a threefold increase in release frequencies led to a proportional increase in firing rate (from  $\sim 10$  to  $\sim 30$  Hz; Fig. 9*B*, ---). Indeed, if all release frequencies were increased by a given factor, the firing rate increased by about the same factor (Fig. 9*C*, □). This shows that, within this range of release frequencies, the average firing rate of the cell reflects the average firing rate of its afferents. However, this relationship was broken if the release frequency was changed only at excitatory synapses: doubling the excitatory release frequency with no change in inhibition tripled the firing rate (Fig. 9*C*, ●).

Surprisingly, in Fig. 9*B* there was only a 12%  $R_{in}$  difference between the 10 and 30 Hz conditions, although the release frequency was threefold higher. This is due to the saturation effect of the  $R_{in}$  change as a function of release frequency (Fig. 3*A1*). This property may explain the observation that visually evoked responses are not paralleled by substantial  $R_{in}$  changes in area 17 neurons (Berman et al. 1991).

Sharp events of lower amplitude than action potentials are also visible in Fig. 9, *A* and *B*. These events are likely to be dendritic spikes that did not reach action potential threshold in the soma/axon region, similar to the fast prepotentials described by Spencer and Kandel (1961). Similar events were reported in intracellular recordings of neocortical pyramidal cells in vivo (Deschênes 1981).

#### Integrative properties during active periods

The dendritic attenuation of EPSPs was examined in the presence of voltage-dependent  $Na^+$  and  $K^+$  dendritic conductances. Using the same stimulation paradigm as in Fig. 6*B*, proximal or distal synapses reliably fired the model cell in quiescent conditions (Fig. 10*A*, Quiet). The stimulation of distal synapses elicited dendritic action potentials that propa-

gated toward the soma in agreement with a previous model (Paré et al. 1998a). During active periods (Fig. 10*A*, Active), proximal or distal stimuli did not trigger spikes reliably although the clustering of action potentials near the time of the stimulation (\*) shows that EPSPs affected the firing probability. The evoked response, averaged from 1,000 sweeps under intense synaptic activity (Fig. 10*A*, Active, avg), showed similar amplitude for proximal or distal inputs. Average responses did not reveal any spiky waveform, indicating that action potentials were not precisely timed with the EPSP in both cases.

It is interesting to note that, in Fig. 10*A*, distal stimuli evoked action potential clustering, whereas proximal stimuli did not, despite the fact that a larger number of proximal synapses were activated. Distal stimuli evoked dendritic action potentials, some of which reached the soma and led to the observed cluster. Increasing the number of simultaneously activated excitatory synapses enhanced spike clustering for both proximal and distal stimuli (Fig. 10*B*, \*). This also was evidenced by the spiky components in the average EPSP (Fig. 10*B*, Active, avg). Comparison of responses evoked by different numbers of activated synapses (Fig. 10*C*) shows that the convergence of several hundred excitatory synapses was necessary to evoke spikes reliably during intense synaptic activity. It is remarkable that with active dendrites, similar conditions of convergence were required for proximal or distal inputs, in sharp contrast to the case with passive dendrites, in which there was a marked difference between proximal and distal inputs (Fig. 6*C*).

The magnitude of the currents active at rest may influence these results. In particular, the significant rectification present at levels more depolarized than  $-60$  mV (Fig. 4*A*) may affect the attenuation of depolarizing events. To investigate this aspect, we estimated the conditions of synaptic convergence using different distributions of leak conductances. Although suppressing the  $I_M$  conductance enhanced the excitability of the cell (see preceding text), it did not affect the convergence requirements in conditions of intense synaptic activity (compare Fig. 11, *A* and *B*). Using a different set of passive parameters based on whole cell recordings, with a low axial resistance and a high membrane resistivity (Pongracz et al. 1991; Spruston and Johnston 1992), also gave similar results (Fig. 11*C*). Using a nonuniform distribution of leak conductance with strong leak in

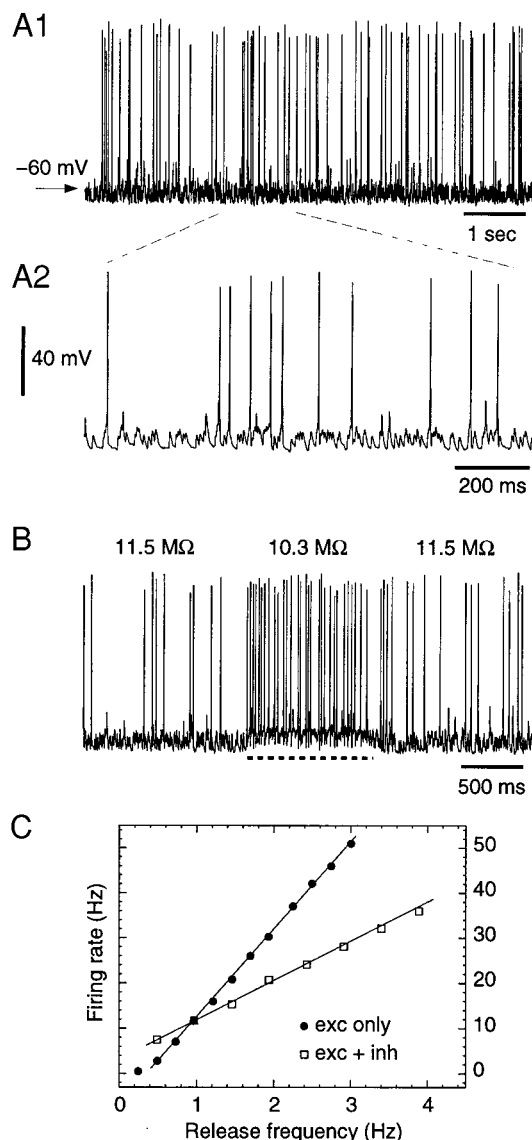


FIG. 9. Tonic firing behavior in simulated active periods. *A1*: in the presence of voltage-dependent  $\text{Na}^+$  and  $\text{K}^+$  conductances distributed in axon, soma, and dendrites, the simulated neuron produced tonic firing at a rate of  $\sim 10$  Hz (action potential threshold of  $-55$  mV,  $\langle V_m \rangle = -65$  mV,  $\sigma_v = 4.1$  mV). *A2*: same simulation as *A1* shown with a faster time base. *B*: effect of a 3-fold increase in release frequency at excitatory and inhibitory synapses. Firing rate of the simulated cell also increased 3-fold (---).  $R_{in}$  is indicated before, during, and after the increase of release frequency. *C*: relation between firing rate and release frequency when the frequency of release was increased at both excitatory and inhibitory synapses ( $\square$ ) or solely at excitatory synapses ( $\bullet$ ).

distal dendrites (Stuart and Spruston 1998) (see METHODS) also led to similar convergence requirements (Fig. 11*D*). In addition, we tested a 10 nS electrode shunt in soma with a larger membrane resistivity in dendrites and obtained nearly identical results (not shown).

These results show that under conditions of intense synaptic activity, synaptic currents account for most of the cell's input conductance, whereas intrinsic leak and voltage-dependent conductances have a comparatively small contribution. It also shows that hundreds of synaptic inputs are required to fire the neuron reliably, and that this requirement seems independent of the location of the synaptic inputs.

## DISCUSSION

The present study provides the first quantitative characterization of the membrane properties of neocortical pyramidal cells in conditions of network activity similar to those observed during the waking state. Intracellular recordings and biophysical models indicated that synaptic activity produces a massive conductance change that is about five times larger than the conductances already present in the cell in the absence of synaptic activity. The model shows that this conductance increase has a major impact on the electrotonic attenuation of EPSPs along the dendritic tree. As this finding might have important implications for understanding how cortical cells process information, we first consider possible pitfalls of our experimental and modeling procedures and then discuss the significance of these findings.

### Possible sources of error

A first possible source of error is that the  $\sim 80\%$  decrease in  $R_{in}$  produced by synaptic activity was observed under anesthesia and a different value might characterize the waking brain. However, the fact that cells fire at similar rates during active periods of ketamine-xylazine anesthesia and during wakefulness indicates that both must be characterized by a similar pattern of synaptic bombardment. This view also is supported by the similar spectral composition of the EEG in these two states.

Two factors might have led us to underestimate the decrease in  $R_{in}$  produced by spontaneous synaptic activity. First, NMDA receptors are antagonized by ketamine, and these channels must reduce further the  $R_{in}$  of cortical cells during the waking state. Second, TTX microperfusion may not have been completely effective in blocking all synapses (although evoked EPSPs were suppressed) (Paré et al. 1997, 1998b), therefore contributing to an additional underestimation of the real  $R_{in}$  change. Ideally, the same analysis should be performed in awake animals, which raises a number of technical difficulties.

Another possible source of error is that the contribution of neuromodulatory currents to the  $R_{in}$  change was not investigated. Most likely, TTX application not only suppresses fast (ionotropic) synaptic activity but also neuromodulatory (metabotropic) influences. Future studies should address this aspect using microperfusion of ionotropic synaptic blockers (NBQX, 2-amino-5-phosphonopentanoic acid, and bicuculline) to estimate the respective contribution of ionotropic and metabotropic activity to the  $R_{in}$  change.

A source of error often raised for sharp-electrode recordings is that the impalement damages the cell. Experimental and modeling evidence suggests that cell damage had a negligible effect on the relative  $R_{in}$  changes measured experimentally. First, blocking spontaneous synaptic activity in vivo using TTX leads to  $R_{in}$  values that are similar to those seen in vitro using the same type of electrodes (Paré et al. 1998b). Second, we report here low  $R_{in}$  values during intense synaptic activity and much larger  $R_{in}$  values after TTX application. These data clearly show that the low  $R_{in}$  of neocortical cells in vivo is not due to cell damage but is attributable to action potential-dependent factors. The marked difference in  $V_m$  before and after TTX also shows that the depolarized  $V_m$  of neocortical cells in vivo is also a consequence of synaptic activity.

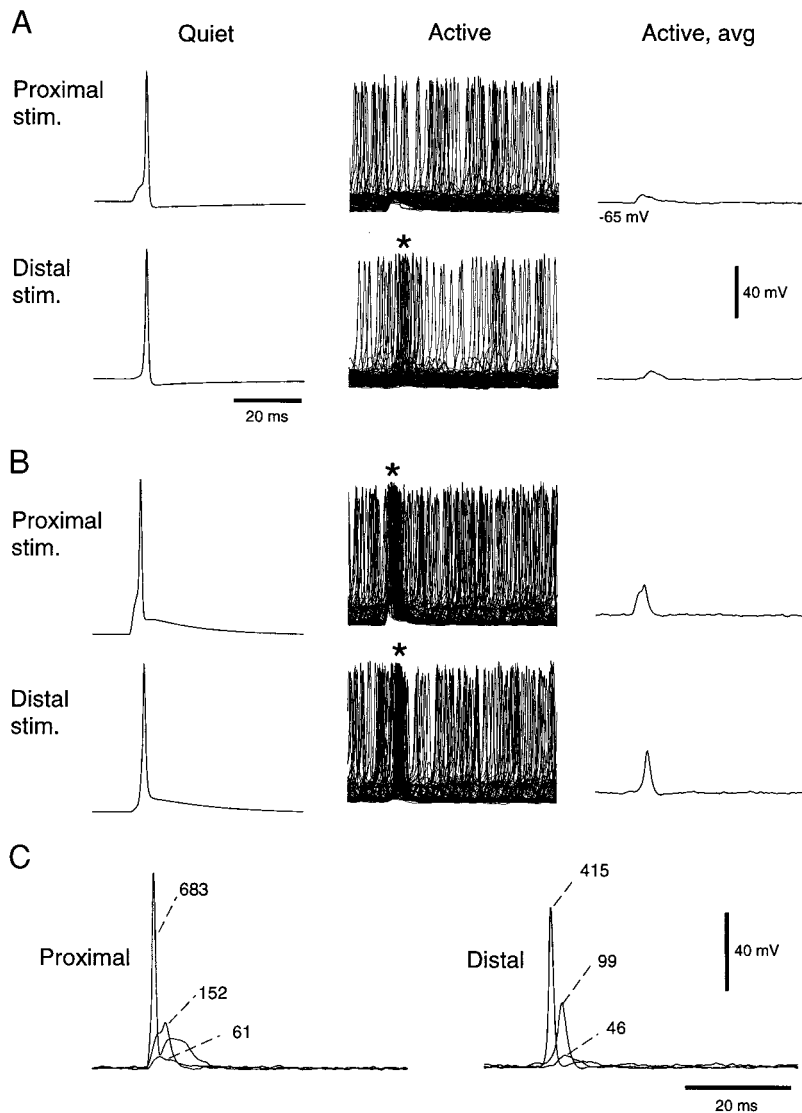


FIG. 10. Attenuation of EPSPs in the presence of voltage-dependent conductances. *A*: same stimulation paradigm as in Fig. 6*B* performed in the presence of  $\text{Na}^+$  and  $\text{K}^+$  currents inserted in axon, soma, and dendrites. Excitatory synapses were activated synchronously in basal ( $n = 61$ ) and distal dendrites ( $n = 46$ ;  $>200 \mu\text{m}$  from soma). In the absence of spontaneous synaptic activity (Quiet), these stimuli reliably evoked action potentials. During simulated active periods (Active; 100 traces shown), the EPSP influenced action potential generation, as shown by the tendency of spikes to cluster for distal stimuli (\*) but not for proximal stimuli. Average responses (Active, avg;  $n = 1,000$ ) shows that action potentials were not precisely timed with the EPSP. *B*: with larger numbers of activated synapses (152 proximal, 99 distal), spike clustering was more pronounced (\*) and the average clearly shows spike-related components. *C*: average response obtained with increasing numbers of synchronously activated synapses. Several hundreds of synapses were necessary to elicit spikes reliably.

The model supports these conclusions by showing that synaptic activity can account for the changes in  $R_{\text{in}}$ ,  $V_m$ , and  $\sigma_v$ . Given that the change in  $R_{\text{in}}$  attributable to synaptic activity was estimated experimentally in the same cells before and after TTX, it is reasonable to assume that the same electrode shunt was present in both conditions. This shunt was included implicitly in the model when adjusting its passive properties (Fig. 2*A*). It also was included explicitly in the model, in combination with higher membrane resistivity, and similar results were obtained. Given that dendritic attenuation is determined essentially by dendritically located conductances, it is not surprising that a simulated electrode shunt in the soma had a minimal effect here.

Another possible source of error is the contribution of voltage-dependent currents that are activated indirectly by synaptic events. In pyramidal neurons, the most numerous ion channels are synaptic: in hippocampal pyramidal cell's dendrites,  $\text{Na}^+$  and  $\text{K}^+$  currents total  $\sim 100\text{--}200 \text{ pS}/\mu\text{m}^2$  (Magee and Johnston 1995; Magee et al. 1998) while AMPA receptors amount to  $\sim 700 \text{ pS}/\mu\text{m}^2$  (assuming 0.6 spines per  $\mu\text{m}^2$ , 1 release site per spine and a quantal conductance of 1,200 pS). The present analysis was based on relatively

hyperpolarized  $V_m$  (less than  $-55 \text{ mV}$ ), as cells were around  $-80 \text{ mV}$  under TTX and in the range of  $-70$  to  $-55 \text{ mV}$  during active periods, with rare excursions above  $-55 \text{ mV}$  (see Fig. 1*F*). In this range of membrane potential, only a small fraction of voltage-dependent channels should be open, whereas a large fraction of ionotropic receptor channels seem to be activated in the conditions studied here. The current-voltage relation was indeed approximately linear in the  $V_m$  range below  $-60 \text{ mV}$  (Fig. 4*A*), suggesting that the  $R_{\text{in}}$  change estimated in this region of  $V_m$  is essentially due to synaptic currents. In addition, simulations indicate that voltage-dependent  $\text{K}^+$  currents contribute  $<10\%$  of the measured  $R_{\text{in}}$  change, even though the model was fit to the cell showing the strongest rectification in our database (Fig. 4). Nevertheless, a significant rectification is present at levels more depolarized than  $-55 \text{ mV}$  (Fig. 4*A*) and should affect the attenuation of depolarizing events. Together, these data indicate that, for  $V_m$ s lower than  $-60 \text{ mV}$ , the conductance due to synaptic activity accounts for most of the  $R_{\text{in}}$  change observed. Further models and experiments are required to investigate if these conclusions are also valid for neurons possessing a prominent  $I_h$  (Stuart and Spruston

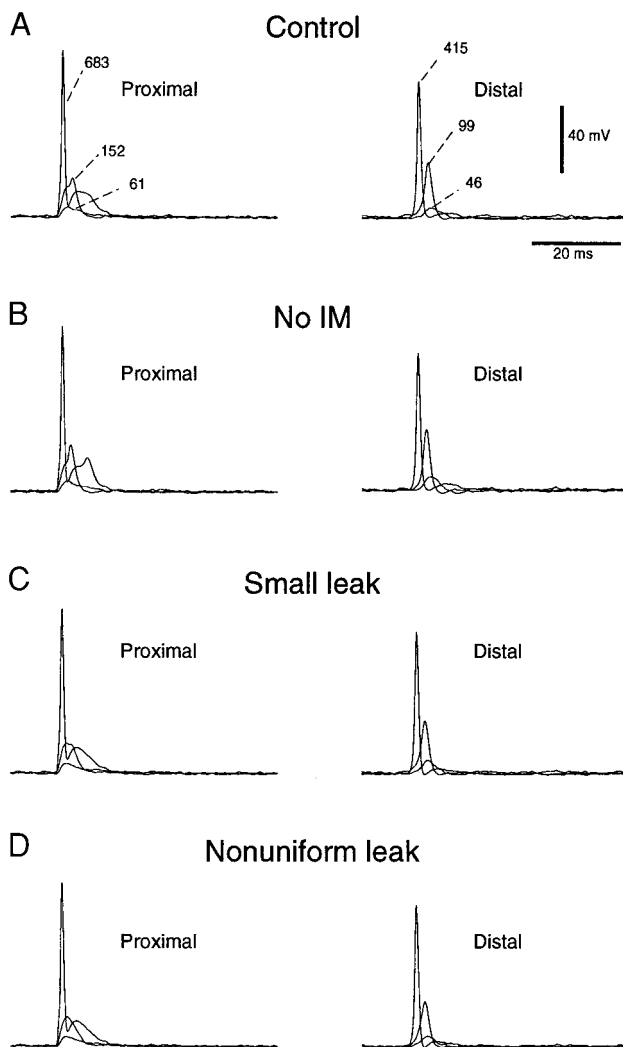


FIG. 11. Synaptic bombardment minimizes the variability due to input location. Average responses to synchronized synaptic stimulation are compared for proximal and distal regions of the dendritic arbor. Same stimulation paradigm as in Fig. 10 repeated for different combination of resting conductances. *A*: control: average response obtained with increasing numbers of synchronously activated synapses (identical simulation as Fig. 10C). *B*: same simulation with  $I_M$  removed. *C*: same simulation as in *A* but with a lower axial resistance ( $100 \Omega\text{cm}$ ) and 3 times lower leak conductance ( $g_{\text{leak}} = 0.015 \text{ mS cm}^{-2}$ ). *D*: same simulation as in *A* with high leak conductance nonuniformly distributed (see METHODS) and low axial resistance ( $80 \Omega\text{cm}$ ).

1998) or prominent calcium and calcium-dependent currents, which may play a role in shaping large depolarizing events.

The lack of constraints is another possible source of error for models. Here, the model was constrained by experimental observations obtained in three conditions of synaptic activity recorded in the same population of cells: absence of synaptic activity (TTX + synaptic blockers), miniature synaptic events (TTX) and intense synaptic activity. For each of these states, the  $R_{\text{in}}$ ,  $V_m$ , and  $\sigma_v$  were calculated, thus providing severe constraints for the model. Indeed, a relatively narrow range of synaptic density, conductance, and release frequency could account for these measurements. However, some parameters were not well constrained. First, there are few or no data available on a possible nonuniform distribution of synaptic

densities, reversal potential, rate of release, correlation of release, as well as the nature, distribution, and kinetics of voltage-dependent currents. These different possibilities should be addressed by future studies as data become available. Second, the axial resistance  $R_i$  could not be constrained. This parameter is usually estimated in the range of  $200\text{--}300 \Omega\text{cm}$  (Rall et al. 1992), but a recent study suggested lower values (Stuart and Spruston 1998). We have tried simulations using  $R_i$  of  $250$  or  $100 \Omega\text{cm}$  and nearly identical results were obtained (Figs. 7C and 11C).

A final source of error is that the models were not simulating the cellular geometries of the recorded neurons. The fact that similar results were obtained using different cellular geometries (Fig. 7) indicates that the exact dendritic morphology was not critical here. However, the dendritic morphology influenced the value of  $\sigma_v$  for equivalent changes in  $R_{\text{in}}$  (Fig. 7B). Future studies should use cellular reconstructions of the recorded cells, allowing more precise simulations of passive properties and of the impact of synaptic currents.

#### Release conditions at cortical synapses

In the suprasylvian cortex of awake cats, neurons display “idle” firing rates of  $\sim 10$  Hz but the rate increases to  $20\text{--}60$  Hz when cells respond to sensory stimuli (Kalaska 1996). In the model, a  $\sim 10$ -Hz firing rate was obtained with release frequencies of  $0.5\text{--}3$  Hz for excitatory synapses and  $4\text{--}8$  Hz for inhibitory synapses. These values are significantly below the reported average firing rate of cortical neurons in this state, suggesting that the release probability of excitatory synapses is significantly less than unity ( $0.025\text{--}0.6$ ). Indeed, in vitro studies indicate a significant decrease in release probability at steady state (Thomson et al. 1993). It should be noted, however, that the estimation of release frequency is dependent of the synaptic density: a twice lower density would require a doubled release frequency to reproduce equivalent results. The present densities were matching the density of spines in rat neocortical dendrites ( $0.6$  spine per  $\mu\text{m}^2$  in Larkman 1991). It is possible that the spine density is lower or higher in cats in which case our estimates of release probability should be revised.

Nevertheless, these release conditions could reproduce the depolarized  $V_m$  and the reduced  $R_{\text{in}}$  evidenced by in vivo experiments. This seemed independent of the exact details of dendritic morphology and cell size (Fig. 7), suggesting that different cells in the neocortex experience similar release conditions during active periods. The model therefore predicts that these changes are generic and are typical of the state of cortical neurons during intense network activity.

In addition to high-frequency release conditions, it was necessary to include a significant correlation among release events to account for experimental measurements. No correlation was necessary to reproduce the characteristics of miniature synaptic potentials, as expected if these events arise from spontaneous release occurring independently at each terminal. On the other hand, an average correlation of  $\sim 0.1$  was necessary to account for the  $V_m$  fluctuations observed during active periods. This is consistent with the average correlation of  $0.12$  measured between pairs of neurons in the cerebral cortex of behaving monkeys (Zohary et al. 1994). The model suggests that this factor, together with the high-frequency release con-

ditions, is sufficient to account for the membrane properties of neocortical cells during active periods. Our results are compatible with the view that during active periods, neocortical cells display weakly correlated discharges ( $c \sim 0.1$ ) (Zohary et al. 1994) occurring at high firing rates ( $\sim 5$ – $20$  Hz) (Evarts 1964; Hubel 1959; Steriade 1978).

#### Implication for dendritic integration

According to cable theory (Rall 1995), dendritic attenuation depends on the membrane conductance. Because our experiments provide evidence for a massive increase of the total membrane conductance during active periods, they predict a major effect on dendritic attenuation, but the exact magnitude of this effect is unknown. The model, constrained by  $R_{in}$ ,  $\langle V_m \rangle$ , and  $\sigma_v$  before and after TTX, revealed drastic effects on dendritic attenuation and that a large number of convergent dendritic synaptic inputs are required to affect the voltage at the soma. By simulating synchronous excitatory synaptic events, it was estimated that the synchronous activation of 80–150 synapses on basal dendrites was necessary for the cell to reach action potential threshold ( $-55$  mV), whereas  $\leq 415$  synapses simulated in distal branches evoked insufficient somatic depolarization (Fig. 6C) or no depolarization at all (Fig. 7C). These simulations show that, because of passive dendritic attenuation, it is difficult for EPSPs arising at distal sites to have a significant effect on the soma if passive properties had to be considered solely.

A very different picture was seen in the presence of dendritic  $Na^+$  and  $K^+$  currents. During intense background synaptic activity, the convergence of hundreds of coincident synaptic inputs was required to evoke spiking reliably (Fig. 10, A–C), similar to the convergence requirements determined with passive dendrites (Fig. 6). However, by contrast with the tremendous attenuation of distal inputs in a passive neuron (Fig. 7C), with active dendrites, the number of synapses required to evoke spiking reliably was approximately the same for proximal and distal stimulation (Fig. 10C). This shows that integrative properties cannot be simply deduced from passive dendritic attenuation. Low-amplitude EPSPs experienced tremendous attenuation because they were subthreshold for the activation of voltage-dependent currents. However, the synchronized stimulation of hundreds of excitatory synapses evoked dendritic action potentials that propagated toward the soma and had an equivalent effect on the firing probability irrespective of their distance from the soma. Active dendrites therefore diminish the variability of the response due to the location of inputs, in agreement with a previous proposition (Cook and Johnston 1997).

The fact that a large number of synchronous synaptic events are required to evoke spiking reliably could suggest that pyramidal cells act like coincidence detectors, as proposed previously (Bernander et al. 1991). However, Fig. 9B also shows that the cell reliably responds to the average firing rate of its afferents. Therefore our experiments and models cannot distinguish between these two possibilities. Rather, our results suggest that, in conditions of intense synaptic activity, pyramidal cells respond reliably only when a very large number of synapses change their release frequency or timing, therefore detecting changes in large populations of neurons.

#### Predictions

The first prediction of this model is that neurons intracellularly recorded in the suprasylvian cortex during the awake state should have markedly reduced  $R_{in}$  (by a  $\geq 5$ -fold factor, see preceding text). This could be tested by performing intracellular recordings in awake animals together with local application of TTX. Although these experiments presently represent a real technical challenge, it is likely that improvements in intracellular recording techniques will make it feasible in the near future.

The second prediction is that a large number of synapses must be activated to influence significantly the probability of action potential generation in neocortical pyramidal neurons in active states. This could be tested using intracellular recordings in ketamine-xylazine anesthesia in a first step and subsequently in awake animals if possible. The convergence criteria could be estimated by using local iontophoresis of increasing amounts of glutamate. The effect on action potentials could be evaluated using similar averaging procedures as shown here. Performing the same experiment under TTX may be used to provide a control of the amplitude/conductance of the evoked EPSPs in the absence of synaptic activity.

The third prediction of the model is that during active periods, similar convergence criteria should be observed for the activation of proximal versus distal synapses. This could be tested using similar paradigms as above by comparing the effect of local glutamate application in deep versus superficial layers of the cortex. The threshold amount of glutamate should be independent of the depth of application.

In conclusion, experiments and models indicate that intense network activity similar to the waking state consists in weakly correlated high-frequency release conditions responsible for a major increase of conductance in pyramidal neurons. The model further indicates that hundreds of highly correlated inputs are required to discharge the cell reliably (Fig. 10C). We suggest that intense network activity maintains pyramidal cells in an idle state during which they are ready to respond rapidly to brief changes of correlation within hundreds of their synaptic inputs. A change of correlation, or synchrony, seems to be the most efficient manner to carry information in these conditions, which supports a possible role for synchronized oscillations in cortical information processing.

This research was supported by the Medical Research Council of Canada and the Natural Science and Engineering Research Council of Canada.

Address for reprint requests: A. Destexhe, Dépt. de Physiologie, Faculté de Médecine, Université Laval, Québec G1K 7P4, Canada.

Received 10 August 1998; accepted in final form 20 November 1998.

#### REFERENCES

- BARRETT, J. N. Motoneuron dendrites: role in synaptic integration. *Fed. Proc.* 34: 1398–1407, 1975.
- BERMAN, N. J., DOUGLAS, R. J., MARTIN, K. A., AND WHITTERIDGE, D. Mechanisms of inhibition in cat visual cortex. *J. Physiol. (Lond.)* 440: 697–722, 1991.
- BERNANDER, O., DOUGLAS, R. J., MARTIN, K. A., AND KOCH, C. Synaptic background activity influences spatiotemporal integration in single pyramidal cells. *Proc. Natl. Acad. Sci. USA* 88: 11569–11573, 1991.
- BUSH, P. AND SEJNOWSKI, T. J. Reduced compartmental models of neocortical pyramidal cells. *J. Neurosci. Methods* 46: 159–166, 1993.

- CONNORS, B. W., GUTNICK, M. J., AND PRINCE, D. A. Electrophysiological properties of neocortical neurons in vitro. *J. Neurophysiol.* 48: 1302–1320, 1982.
- CONTRERAS, D., DESTEXHE, A., AND STERIADE, M. Intracellular and computational characterization of the intracortical inhibitory control of synchronized thalamic inputs in vivo. *J. Neurophysiol.* 78: 335–350, 1997.
- CONTRERAS, D., TIMOFEEV, I., AND STERIADE, M. Mechanisms of long lasting hyperpolarizations underlying slow sleep oscillations in cat corticothalamic networks. *J. Physiol. (Lond.)* 494: 251–264, 1996.
- COOK, E. P. AND JOHNSTON, D. Active dendrites reduce location-dependent variability of synaptic input trains. *J. Neurophysiol.* 78: 2116–2128, 1997.
- CRAGG, B. G. The density of synapses and neurones in the motor and visual areas of the cerebral cortex. *J. Anat.* 101: 639–654, 1967.
- DEFELIPE, J. AND FARIÑAS, I. The pyramidal neuron of the cerebral cortex: morphological and chemical characteristics of the synaptic inputs. *Prog. Neurobiol.* 39: 563–607, 1992.
- DESCHÊNES, M. Dendritic spikes induced in fast pyramidal track neurons by thalamic stimulation. *Exp. Brain Res.* 43: 304–308, 1981.
- DESTEXHE, A., CONTRERAS, D., STERIADE, M., SEJNOWSKI, T. J., AND HUGUENARD, J. R. In vivo, in vitro and computational analysis of dendritic calcium currents in thalamic reticular neurons. *J. Neurosci.* 16: 169–185, 1996.
- DESTEXHE, A., MAINEN, Z. F., AND SEJNOWSKI, T. J. An efficient method for computing synaptic conductances based on a kinetic model of receptor binding. *Neural Comput.* 6: 14–18, 1994.
- DESTEXHE, A., MAINEN, Z. F., AND SEJNOWSKI, T. J. Kinetic models of synaptic transmission. In: *Methods in Neuronal Modeling* (2nd ed.), edited by C. Koch and I. Segev. Cambridge, MA: MIT Press, 1998, p. 1–26.
- DOUGLAS, R. J., MARTIN, K. A., AND WHITTERIDGE, D. An intracellular analysis of the visual responses of neurones in cat visual cortex. *J. Physiol. (Lond.)* 440: 659–696, 1991.
- EVARTS, E. V. Temporal patterns of discharge of pyramidal tract neurons during sleep and waking in the monkey. *J. Neurophysiol.* 27: 152–171, 1964.
- FARIÑAS, I. AND DEFELIPE, J. Patterns of synaptic input on corticocortical and corticothalamic cells in the visual cortex. I. The cell body. *J. Comp. Neurol.* 304: 53–69, 1991a.
- FARIÑAS, I. AND DEFELIPE, J. Patterns of synaptic input on corticocortical and corticothalamic cells in the visual cortex. II. The axon initial segment. *J. Comp. Neurol.* 304: 70–77, 1991b.
- FATT, P. Sequence of events in synaptic activation of a motoneurone. *J. Neurophysiol.* 20: 61–80, 1957.
- GRUNER, J. E., HIRSCH, J. C., AND SOTELO, C. Ultrastructural features of the isolated suprasylvian gyrus. *J. Comp. Neurol.* 154: 1–27, 1974.
- HINES, M. L. AND CARNEVALE, N. T. The NEURON simulation environment. *Neural Comput.* 9: 1179–1209, 1997.
- HOFFMAN, D. A., MAGEE, J. C., COLBERT, C. M., AND JOHNSTON, D. A. K<sup>+</sup> channel regulation of signal propagation in dendrites of hippocampal pyramidal neurons. *Nature* 387: 869–875, 1997.
- HOLMES, W. R. AND WOODY, C. D. Effects of uniform and non-uniform synaptic “activation-distributions” on the cable properties of modeled cortical pyramidal neurons. *Brain Res.* 505: 12–22, 1989.
- HUBEL, D. Single-unit activity in striate cortex of unrestrained cats. *J. Physiol. (Lond.)* 147: 226–238, 1959.
- HUGUENARD, J. R., HAMILL, O. P., AND PRINCE, D. A. Developmental changes in Na<sup>+</sup> conductances in rat neocortical neurons: appearance of a slowly inactivating component. *J. Neurophysiol.* 59: 778–795, 1988.
- KALASKA, J. F. Parietal cortex area 5 and visuomotor behavior. *Can. J. Physiol. Pharmacol.* 74: 483–498, 1996.
- KOCH, C., RAPP, M., AND SEGEV, I. A brief history of time (constants). *Cereb. Cortex* 6: 93–101, 1996.
- LARKMAN, A. U. Dendritic morphology of pyramidal neurons of the visual cortex of the rat. III. Spine distributions. *J. Comp. Neurol.* 306: 332–343, 1991.
- LLINÁS, R. AND NICHOLSON, C. Electrophysiological properties of dendrites and somata in alligator Purkinje cells. *J. Neurophysiol.* 34: 532–551, 1971.
- MAGEE, J. C., HOFFMAN, D., COLBERT, C., AND JOHNSTON, D. Electrical and calcium signalling in dendrites of hippocampal pyramidal neurons. *Annu. Rev. Physiol.* 60: 327–346, 1998.
- MAGEE, J. C. AND JOHNSTON, D. Characterization of single voltage-gated Na<sup>+</sup> and Ca<sup>2+</sup> channels in apical dendrites of rat CA1 pyramidal neurons. *J. Physiol. (Lond.)* 487: 67–90, 1995.
- MAINEN, Z. F., JOERGES, J., HUGUENARD, J. R., AND SEJNOWSKI, T. J. A model of spike initiation in neocortical pyramidal neurons. *Neuron* 15: 1427–1439, 1995.
- MARKRAM, H., LÜBKE, J., FROTSCHER, M., RODTH, A., AND SAKMANN, B. Physiology and anatomy of synaptic connections between thick tufted pyramidal neurones in the developing rat neocortex. *J. Physiol. (Lond.)* 500: 409–440, 1997.
- MASON, A., NICOLL, A., AND STRATFORD, K. Synaptic transmission between individual pyramidal neurons of the rat visual cortex in vitro. *J. Neurosci.* 11: 72–84, 1991.
- MCCORMICK, D. A. AND PRINCE, D. A. Mechanisms of action of acetylcholine in the guinea-pig cerebral cortex in vitro. *J. Physiol. (Lond.)* 375: 169–194, 1986.
- MUNGAI, J. M. Dendritic patterns in the somatic sensory cortex of the cat. *J. Anat.* 101: 403–418, 1967.
- PARÉ, D., LANG, E. J., AND DESTEXHE, A. Inhibitory control of somatic and dendritic sodium spikes in neocortical pyramidal neurons in vivo: an intracellular and computational study. *Neuroscience* 84: 377–402, 1998a.
- PARÉ, D., LEBEL, E., AND LANG, E. J. Differential impact of miniature synaptic potentials on the somata and dendrites of pyramidal neurons in vivo. *J. Neurophysiol.* 78: 1735–1739, 1997.
- PARÉ, D., SHINK, E., GAUDREAU, H., DESTEXHE, A., AND LANG, E. J. Impact of spontaneous synaptic activity on the resting properties of cat neocortical neurons in vivo. *J. Neurophysiol.* 79: 1450–1460, 1998b.
- PONGRACZ, F., FIRESTEIN, S., AND SHEPHERD, G. M. Electrotone structure of olfactory sensory neurons analyzed by intracellular and whole cell patch techniques. *J. Neurophysiol.* 65: 747–758, 1991.
- PRESS, W. H., FLANNERY, B. P., TEUKOLSKY, S. A., AND VETTERLING, W. T. *Numerical Recipes*. Cambridge, UK: Cambridge Univ. Press, 1986.
- RALL, W. *The Theoretical Foundation of Dendritic Function*, edited by I. Segev, J. Rinzel, and G. M. Shepherd. Cambridge, MA: MIT Press, 1995.
- RALL, W., BURKE, R. E., HOLMES, W. R., JACK, J. J., REDMAN, S. J., AND SEGEV, I. Matching dendritic neuron models to experimental data. *Physiol. Rev.* 72: S159–S186, 1992.
- SALIN, P. AND PRINCE, D. A. Spontaneous GABA<sub>A</sub> receptor-mediated inhibitory currents in adult rat somatosensory cortex. *J. Neurophysiol.* 75: 1573–1587, 1996.
- SPAIN, W. J., SCHWINDT, P. C., AND CRILL, W. E. Anomalous rectification in neurons from cat sensorimotor cortex in vitro. *J. Neurophysiol.* 57: 1555–1576, 1987.
- SPENCER, W. A. AND KANDEL, E. R. Electrophysiology of hippocampal neurons. IV. Fast prepotentials. *J. Neurophysiol.* 24: 272–285, 1961.
- SPRUSTON, N. AND JOHNSTON, D. Perforated patch-clamp analysis of the passive membrane properties of three classes of hippocampal neurons. *J. Neurophysiol.* 67: 508–529, 1992.
- STAFSTROM, C. E., SCHWINDT, P. C., AND CRILL, W. E. Negative slope conductance due to a persistent subthreshold sodium current in cat neocortical neurons in vitro. *J. Brain Res.* 236: 221–226, 1982.
- STERN, P., EDWARDS, F. A., AND SAKMANN, B. Fast and slow components of unitary EPSCs on stellate cells elicited by focal stimulation in slices of rat visual cortex. *J. Physiol. (Lond.)* 449: 247–278, 1992.
- STERIADE, M. Cortical long-axoned cells and putative interneurons during the sleep-waking cycle. *Behav. Brain Sci.* 3: 465–514, 1978.
- STERIADE, M., AMZICA, F., AND NUÑEZ, A. Cholinergic and noradrenergic modulation of the slow (~0.3 Hz) oscillation in neocortical cells. *J. Neurophysiol.* 70: 1384–1400, 1993a.
- STERIADE, M., NUÑEZ, A., AND AMZICA, F. A novel slow (<1 Hz) oscillation of neocortical neurons in vivo: depolarizing and hyperpolarizing components. *J. Neurosci.* 13: 3252–3265, 1993b.
- STUART, G., DODT, H. U., AND SAKMANN, B. Patch clamp recording from the soma and dendrites of neurons in brain slices using infrared video microscopy. *Pflügers Arch.* 423: 511–518, 1993.
- STUART, G. J. AND SAKMANN, B. Active propagation of somatic action potentials into neocortical pyramidal cell dendrites. *Nature* 367: 69–72, 1994.
- STUART, G., SCHILLER, J., AND SAKMANN, B. Action potential initiation and propagation in rat neocortical pyramidal neurons. *J. Physiol. (Lond.)* 505: 617–632, 1997.
- STUART, G. AND SPRUSTON, N. Determinants of voltage attenuation in neocortical pyramidal neuron dendrites. *J. Neurosci.* 18: 3501–3510, 1998.
- SZENTAGOTHAÏ, J. The use of degeneration in the investigation of short neuronal connections. In: *Progress in Brain Research*, edited by M. Singer and J. P. Shade. Amsterdam: Elsevier, 1965, vol. 14, p. 1–32.

- THOMSON, A. M. AND DEUCHARS, J. Synaptic interactions in neocortical local circuits: dual intracellular recordings in vitro. *Cereb. Cortex* 6: 510–522, 1997.
- THOMSON, A. M., DEUCHARS, J., AND WEST, D. C. Large, deep layer pyramidal single axon EPSPs in slices of rat motor cortex display paired pulse and frequency-dependent depression, mediated presynaptically and self-facilitation, mediated postsynaptically. *J. Neurophysiol.* 70: 2354–2369, 1993.
- TRAUB, R. D. AND MILES, R. *Neuronal Networks of the Hippocampus*. Cambridge, UK: Cambridge Univ. Press, 1991.
- WHITE, E. L. *Cortical Circuits*. Boston, MA: Birkhauser, 1989.
- WONG, R.K.S., PRINCE, D. A., AND BASBAUM, A. I. Intradendritic recordings from hippocampal neurons. *Proc. Natl. Acad. Sci. USA* 76: 986–990, 1979.
- YUSTE, R. AND TANK, D. W. Dendritic integration in mammalian neurons, a century after Cajal. *Neuron* 16: 701–716, 1996.
- ZOHARY, E., SHADLEN, M. N., AND NEWSOME, W. T. Correlated neuronal discharge rate and its implications for psychophysical performance. *Nature* 370: 140–143, 1994.